Sap flow responses in pioneer and late-successional tree species in secondary tropical montane forests of Eastern Himalaya, India

Manish Kumar[a,b,c*], Gladwin Joseph[a,d], Yangchenla Bhutia[a,b,e] and Jagdish Krishnaswamy[a,b,f]

[a]Ashoka Trust for Research in Ecology and the Environment (ATREE), Bangalore 560064, India.

[b]Manipal Academy of Higher Education (MAHE), Manipal 576104, Karnataka, India.

[c]School of Geography, Earth and Environmental Sciences, University of Birmingham, B15 2TT, UK.

[d]Conservation Biology Institute, Oregon 97333, USA.

[e]Sikkim State Council of Science & Technology, Gangtok 737102, India.

[f]School of Environment and Sustainability, Indian Institute for Human Settlements, Bangalore 560080, India.

*Corresponding author: Manish Kumar

Corresponding author's contact information

Dr Manish Kumar

311, LES Building, School of Geography, Earth and Environmental Sciences, University of Birmingham, B15 2TT, UK

ORCID: 0000-0002-6780-9336

Primary email id: m.kumar.2@bham.ac.uk

Secondary email id: manish.kumar@atree.org

Phone Number: +447500758000

Co-author's Email id:

gladwin.joseph@consbio.org; yangchenla.bhutia@atree.org; jkrishnaswamy@iihs.ac.in

Highlights

First reports of contrasting and interactive water use strategies among co-occurring pioneers and late-successional tree species with significant nocturnal sap flow from secondary Eastern Himalayan tropical montane forests in India.

Abstract

The interactive role of life-history traits and environmental forcing on plant-water relations is crucial for understanding species response to climate change but remains poorly understood in secondary tropical montane forests (TMFs). Comparing contrasting life-history traits (pioneer vs late-successional species) in a biodiverse Eastern Himalayan secondary TMF, we investigated sap flow responses in co-occurring pioneer species, *Symplocos racemosa* (n=5) and *Eurya acuminata* (n=5), and late-successional species, *Castanopsis hystrix* (n=3), using modified Granier's Thermal Dissipation probes. The fast-growing pioneers *S. racemosa* and *E. acuminata*) had 2.1- and 1.6-times higher sap flux density than the late-successional *C. hystrix*, respectively, and exhibited characteristics of long-lived pioneer species. Significant radial and azimuthal variability in sap flow (V) between species was observed and attributed to life history traits and the canopy's access to sunlight. Nocturnal V (1800-0500 hr) was 13.8 % of daily V and is attributed to stem recharge for evening V (1800-2300 hr) and to endogenous stomatal controls for pre-dawn V (0000-0500 hr). Both the shallow-rooted pioneer species exhibited midday depression in V attributed to photosensitivity and diel moisture stress response. In contrast, deep-rooted *C. hystrix* transpired unaffected across the dry season likely accessing groundwater. Thus, the secondary broadleaved TMFs, with the dominance of shallow-rooted pioneers, are more prone to the negative impacts of drier and warmer winters than primary forests, which are dominated by deep-rooted species. The study provides an empirical understanding of life-history traits and microclimate modulating plant-water use in widely distributed secondary TMFs in Eastern Himalaya and highlights their vulnerability against warmer winters and reduced snowfall due to climate change.

Keywords

Sap flow, Transpiration, Pioneer, Late-successional, Plant Water relations, Secondary Forests, Ecohydrology, Himalaya

Abbreviations

ACF - Autocorrelation Coefficient; AIC - Akaike information criterion; ANOVA - Analysis of variance; APHRODITE - Asian Precipitation-Highly Resolved Observational Data Integration Towards Evaluation of Water Resources; AWS - Automatic Weather Station; corARMA - Second-order AutoRegressive Moving Average; CV - Coefficients of Variability; GLS - Generalized least squares; KGE - Kling- Gupta Efficiency; MAP - Mean Annual Precipitation; masl - Meters above sea level; MLRM - Multiple Linear Regression Models; RCP - Representative Concentration Pathway; SPAC - Soil-Plant-Atmosphere-Continuum; TDP - Thermal Dissipation Probes; TMF - Tropical Montane Forests; VPD - Vapour Pressure Deficit.

Graphical Abstract

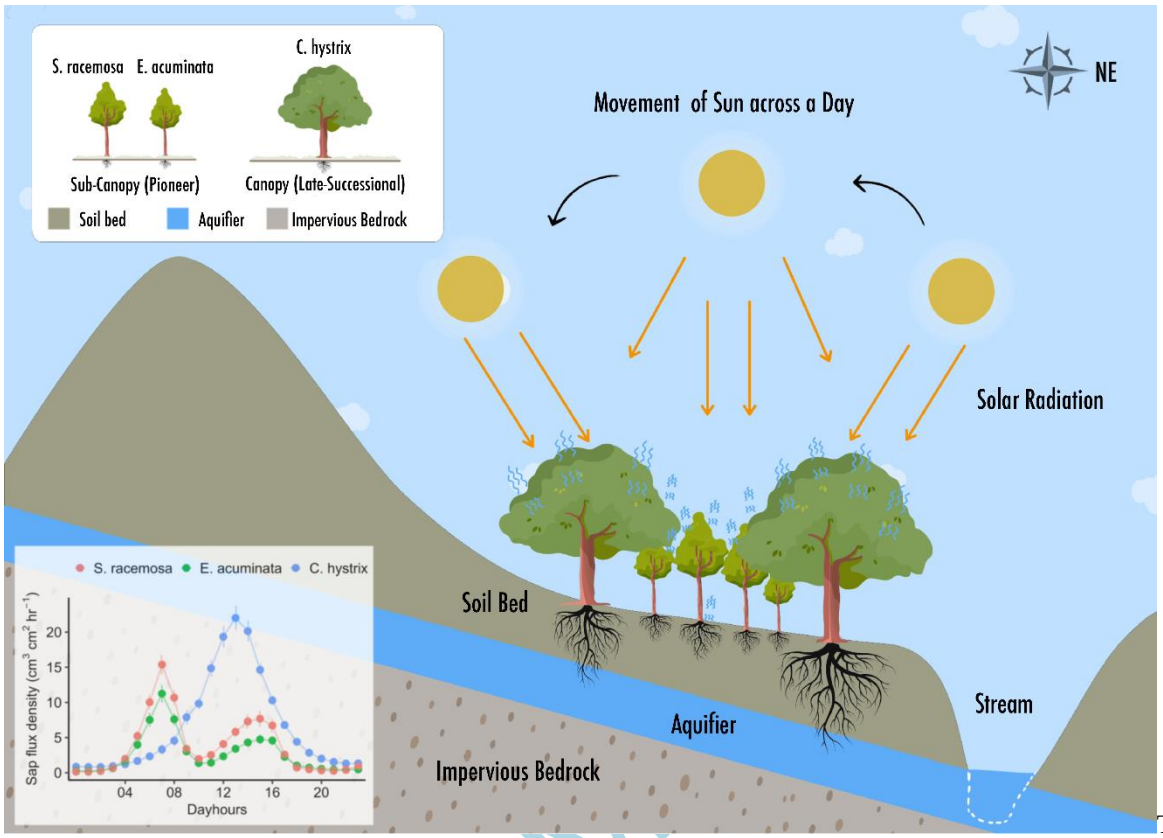

The access to soil moisture and sunlight dictates diurnal sap flux density (J in cm3 cm-2 h-1) patterns among co-occurring pioneer and emergent species in a secondary tropical montane forest in Eastern Himalaya (The image is not to scale and requires colour print).

Introduction

Plant-water relations play a crucial role in modulating carbon and water fluxes in recovering secondary tropical forests. In most terrestrial systems, the availability of energy and water are the primary drivers of water-use by vegetation, mainly through transpiration (Heimann and Reichstein, 2008; Asbjornsen *et al.*, 2011). Transpiration is the movement of water from the soil to the atmosphere via the stem, based on a gradient of total water potential along the Soil-Plant-Atmosphere-Continuum (SPAC), an active area of research in ecohydrology (Asbjornsen *et al.*, 2011; Manzoni *et al.*, 2013; Mencuccini *et al.*, 2019). Transpiration is driven by environmental variables like Vapour Pressure Deficit (VPD), an index of atmospheric dryness, light and soil moisture availability, and ecophysiological traits controlling plant water-use such as wood anatomy, rooting depth, stomatal density, and sapwood density (Asbjornsen *et al.*, 2011; Manzoni *et al.*, 2013). These ecophysiological traits have evolved through competition and adaptation between co-occurring species belonging to different functional groups (pioneer or late-successional) and contribute to the inter-specific variability in sap flow (between individuals of different species) (O'Brien *et al.*, 2004; Hernandez-Santana *et al.*, 2015). Research typically divides the inter-specific variation along the fast-slow/growth-survival axes, where pioneer species tend to adopt a 'live fast and die young' approach to maximise growth (with high plant-water use), while climax or late-successional species prefer low-risk, slow growth (with conservative water-use) and high survival rates (Rüger *et al.*, 2020; Lai *et al.*, 2021).

The intra-specific (within individuals of the same species) variations manifest as radial and azimuthal (between cardinal directions) variability in sap flow and are influenced by growth stages, size, stem anatomy (ring-porous vs. diffuse-porous species), and individual responses to the microclimate (Fiora and Cescatti, 2006; Berdanier *et al.*, 2016; Berry *et al.*, 2018). Thus, individual and species-level studies are crucial for understanding the responses of co-occurring species belonging to similar or different functional groups, against changing environmental conditions, especially in bio-diverse tropical montane forests (TMFs) (Forrester, 2015; Bretfeld *et al.*, 2018; Basnett and Devy, 2021). Such studies are also crucial to our understanding of the responses of secondary forest communities to the predicted intensification of the hydrological cycle with climate change, especially against extreme precipitation events, seasonal droughts and reducing winter precipitation (Donohue *et al.*, 2007; Zeppel *et al.*, 2008, 2011; Kulkarni *et al.*, 2013; Bretfeld *et al.*, 2018). The impact of atmospheric CO2 fertilization on plant-water use and carbon assimilation rates, and subsequently on the carbon sequestration potential, is another important area of research from TMFs (Bugmann and Bigler, 2011; Eckert *et al.*, 2021).

However, ecohydrological studies describing linkages between micro-environment and ecophysiological traits associated with transpiration, and their underlying mechanisms, are relatively sparse in TMFs. Most such studies are restricted to the tropical Andes and South-East Asia, and very little research has come from the Himalaya (Bruijnzeel *et al.*, 2011; Poyatos *et al.*, 2021). In Himalaya, the studies on plant-water relations have mainly focused on inter-specific patterns in leaf water potential with environmental gradients, most coming from the drier and relatively higher latitude Western Himalaya (Poudyal et al., 2004; Singh et al., 2006; Zobel & Garkoti, 2001). Direct measurements of whole-tree transpiration are rare, with Ghimire et al. (2014) being the first to compare the variability in transpiration rates between needle-leaved Chir pine (*Pinus roxburghii*) and broad-leaved Oak forests in Central Himalaya using sap flow probes. Previous studies have also highlighted the crucial role of seasonal soil moisture fluctuations on phenology and growth cycles in broad-leaved trees in the Himalaya (Singh *et al.*, 2000; Tewari *et al.*, 2016; Chand *et al.*, 2017). Others have explored the variability in the ecophysiological responses of Himalayan trees to seasonal moisture deficit across elevation, species range and canopy structure (Zobel *et al.*, 2001; Singh *et al.*, 2006*b*; Tewari *et al.*, 2018). The majority of broad-leaved TMFs in the Himalaya are secondary forests due to the long history of human forest use and remain understudied (Ramakrishnan and Kushwaha, 2001; Kanade and John, 2018). Secondary TMFs differ significantly from their primary counterparts in having co-existing different successional stages like pioneer species and late-successional species and mixed stand structure (sub-canopy and emergent trees) (Ramakrishnan and Kushwaha, 2001; Nogueira *et al.*, 2004). A third of the total forest cover in Sikkim, secondary TMFs form a significant carbon sink and provide sanctuary to the principal water resources, the springs and streams (Wohl *et al.*, 2012; Brown *et al.*, 2019; Daniel *et al.*, 2021; Kumar *et al.*, 2023). A majority of these forests are under protected area management, and thus understanding their plant-water relations is critical to the water and ecological security of the Eastern Himalaya (Kanade and John, 2018). The region is threatened by the projections of a high rate of warming (+5°C), precipitation changes (+40%) and loss of biodiversity (33 %) by the end of the 21st century under climate change (Kulkarni *et al.*, 2013; Krishnan *et al.*, 2019; Dahal *et al.*, 2021). Furthermore, the forests in parts of the Himalaya have shown browning trends in response to warming-induced moisture stress in recent decades (Krishnaswamy *et al.*, 2014), thus making a better understanding of plant-water relations a research priority.

However, to the best of our knowledge, plant-water relations or transpiration have not been studied in the wet secondary TMFs of Eastern Himalaya using direct whole-tree methods such as sap flow. Further, the variability in water-use strategies among different functional groups in response to moist and seasonally dry conditions,

and its impact on plant productivity and carbon sequestration potential of these human-dominated biodiverse forest communities remains yet to be explored (Bretfeld *et al.*, 2018). The study addresses the knowledge gap using a response-based approach to understand the variability in plant water use among co-occurring functional groups, pioneer species and late-successional species to micro-meteorological and environmental forcing under the SPAC framework (Mencuccini *et al.*, 2019; Kannenberg *et al.*, 2022). Specifically, the study addresses two main questions in an East Himalayan broad-leaved wet evergreen TMF: (A) How do the sap flow patterns differ between co-occurring pioneer and late-successional species in a secondary forest? and (B) What are the environmental and ecophysiological drivers of variability in sap flow responses? We hypothesize that the plant-water use by the pioneer species would be high but equally likely to be highly sensitive to environmental extremes, whereas late-successional species will have relatively stable water-use patterns. We also predict that, unlike other TMFs, the ecosystem productivity is more likely to be limited by energy availability than water in the wet East Himalayan eco-climate.

Materials and methods

1.1. Experimentation site and forest stand description

The forest stand represents the East Himalayan broad-leaved evergreen wet montane forest classification (Sudhakar *et al.*, 2008; Kanade and John, 2018; Bhutia *et al.*, 2019). The study site is unique in being the wettest (mean annual precipitation (MAP) of 4650±120 mm) high-elevation (> 2000 masl, meters above sea level) tropical montane forest site in the world, where direct sap flow-based plant water flow measurements have been carried out so far (Bruijnzeel *et al.*, 2011; Poyatos *et al.*, 2021). These tropical montane forests are distinguished from the temperate broadleaved evergreen forests (high latitude and low elevation) in terms of being closer to the tropics (20°-35° N), high elevation (800-2800 masl), a wet/humid climate (3000-5000 mm annual rainfall), moderate energy conditions (12 °C mean annual temperature) and high biodiversity (Ohsawa, 1993; Tang and Ohsawa, 1999; Kanade and John, 2018). The field experiment was conducted in an early successional secondary forest stand (27.35° N, 88.56° E) in the Fambong-Lho Wildlife Sanctuary (FWS), Sikkim, with the annual daily average temperature ranging from -2 to 24 °C. The hydrologic year is divided into three distinct seasons: Summer (March to May), characterized by warm days, cloudy afternoons, significant pre-monsoon precipitation, and high evapotranspiration; Monsoon (June to October) with concentrated precipitation, high humidity, and low evapotranspiration; and Winter (November to February) with sunny days, cold nights,

occasional snowfall and moderate evapotranspiration (Kumar *et al.*, 2021). The forest is sloped at 10°-35°, predominantly facing the northeast direction, and the soil is well-drained sandy-loam with moderate soil depth (40-100 cm).

The vegetation data were derived from five 100 m X 10 m vegetation surveys recording 321 trees of 16 species belonging to 12 families (Bhutia *et al.*, 2019). The composition marks the stand as an early-successional secondary forest with a short-statured canopy dominated by pioneer species like *Symplocos spp* and *Eurya spp*. The older, taller and large-girthed individuals of the Fagaceae family, such as *Castanopsis spp* and *Quercus spp*, stand out as emergent trees (Sudhakar *et al.*, 2008; Bhutia *et al.*, 2019; Gurung and Chettri, 2019). Tree density was a better estimate for understanding the population structure of pioneer species than basal area because of the higher number of small-sized individuals, whereas the late-successional species were large-sized and fewer in numbers. The selection of species for sap flow instrumentation was based on: (1) representation of the successional stages (pioneer and late-successional), and (2) selection of dominant species in each of the successional stages based on the tree density and basal area distribution of the forest stand. The selected species, *Symplocos racemosa* and *Eurya acuminata*, represent the fast-growing pioneer species community, whereas *Castanopsis hystrix* was the most dominant species belonging to the climax or late-successional stage (Supplementary Figure S1A and S1B for the tree density and basal area, respectively). Table 1 summarises the information on rooting depth, phenology, and other ecophysiological characteristics of the three species collated from available literature and personal observations (Ohsawa *et al.*, 1986; Suzuki *et al.*, 1991; Sundriyal and Sharma, 1996, 2003; Chettri *et al.*, 2002; Sharma *et al.*, 2011; Li *et al.*, 2013). *S. racemosa* was observed to be flowering and fruiting during the monsoon (June - July). *E. acuminata* flowered at the peak of the dry season in December-January and fruited during February-March. *C. hystrix* flowered in February and fruited in March-April. The three species did not have any concentrated leaf fall (personal observations).

Table 1. Life forms and ecophysiological characteristics of the three studied species.

1.2. Sap flux measurements

Sapwood thickness was measured from wood cores extracted using an increment borer from each instrumented tree at the start of instrumentation (14th December 2013). Wood cores from *C. hystrix* showed

distinct heartwood formation and only the outer xylem (4-5 cm) was observed to be functional. No heartwood was detected in *S. racemosa* and *E. acuminata*, and the entire xylem was assumed functional, a characteristic of diffuse-porous species (Berdanier *et al.*, 2016). The sapwood cores were wrapped in plastic clingwrap at the site to avoid moisture loss and processed in the laboratory. Each core was cut into 1 cm long sections to estimate wood density and moisture following Chave (2006). Sap flux measurements were carried out between November 2013 to May 2014 in 13 trees, five trees each of *S. racemosa* and *E. acuminata*, and three trees of *C. hystrix*, using Granier's thermal dissipation method-based probes (TDPs) (Table 2) (Granier, 1987; Lu *et al.*, 2004). The sample size of 13 trees is at par with the average number of trees sampled in sap flow studies globally, and the installation design was optimized to cover maximum xylem variability (Asbjornsen *et al.*, 2011; Guyot *et al.*, 2015). Davis et al. (2012) suggested modifications to the lab-built TDP design template to measure sap flow at the top one centimetre of the probe and validated the lab-built probes against the commercial Dynamax TDP30 sap flow probe. The study followed the modified design template to lab-build the TDP probes (for further details, see Phillips et al. 1996, James et al. 2002, Harmon 2009, Davis et al. 2012). TDP are the most widely used sap flow technique across the globe and perform well in cold and low-flow conditions (Lu *et al.*, 2004; Chan and Bowling, 2017; Wang *et al.*, 2023), but also show linear systemic bias and thus are suitable for relative comparison between species (Peters *et al.*, 2018; Flo *et al.*, 2019). Radial probes of 1-5 cm length were installed at one-centimetre incremental depths (10, 20, 30, 40, and 50 mm) from the cambium in one tree per species (henceforth referred to as radial trees), respectively, in a spiral design. The remaining trees per species (henceforth referred to as replicate trees) were fitted with two 2-cm length probes installed in the north and south aspects to observe azimuthal variability (Shinohara *et al.*, 2013; Komatsu *et al.*, 2016). A design limitation of using multiple sap flow probes of different depths in a spiral is the potentially confounding interactions between radial and circumferential variability, which can induce significant biases in whole-tree water use, especially in trees with non-uniform xylem growth patterns (James *et al.*, 2002).

Table 2. Biometric details (± standard deviation), the total number of data days and the number of radial probes installed per tree for the three species.

The probe signals (in millivolts) were converted to temperature difference (ΔT in °C) between the heater and reference probes and stored in a multi-channel data logger (DL2e, Delta-T, UK). The zero-sap flow

assumption, at which the temperature difference between the probes is maximum (ΔT_{max}), is critical for Granier's method and a significant source of error in TDP-based sap flow estimation. Comparing different approaches to determining ΔT_{max}, Rabbel et al. (2016) show that daily ΔT_{max} has lower variability than studies using moving-window or regression-based approaches and recommended daily ΔT_{max} for research in humid environments without significant water limitations. Thus, sap flux density (J, $cm^3\ cm^2\ hr^{-1}$) was computed following Granier's empirical equation (equation 1), where ΔT_{max} was determined daily for each probe. After due quality checks, 114 days of sap flow data were used for the final analysis, including 33 days where data was present for all three species (Table 2, Supplementary Figure S2). The first two weeks of data were ignored to avoid sap flux errors due to installation wounds (Wiedemann *et al.*, 2016).

$$J = 119 * 10^{-6} * 3600 * \left(\frac{(\Delta T_{max} - \Delta T)}{\Delta T}\right)^{1.231} \quad (1)$$

1.3. Environmental measurements

Soil water potential was recorded at 10 cm incremental depths from the surface at 10 min resolution using granular matrix-based (watermark) sensors (Virtual Electronics, Roorkee) and converted to volumetric water content using the site-specific van Genuchten water retention curve parameters. The curve parameters were developed using the percentage of soil organic matter and organic carbon, particle size distribution (sand, silt, and clay), bulk density and porosity as input parameters to the Rosetta software (Schaap *et al.*, 2001). The hourly total soil moisture (S in mm) for the topsoil (0-30 cm depth) was computed using the trapezoidal method and smoothened using a 3-step moving-average window to gap-fill stray missing values (Nachabe *et al.*, 2005). In-canopy air temperature and relative humidity were recorded at 10 mins resolution (iButton Hygrochrons, Maxim Int., USA). Air temperature (°C), relative humidity (R_h in %), wind speed (u in m s^{-1}), and incoming short-wave radiation (R_s in kW m^{-2}, henceforth referred to as solar radiation) were recorded 10 mins resolution using an automatic weather station (AWS) (Vantage-pro Davis Net, USA). Vapour pressure deficit (VPD, kPa) was calculated from the hourly air temperature and relative humidity observed by the Hygrochrons and the AWS and averaged. Precipitation (P in mm h^{-1}) was recorded using an automated tipping-bucket rain gauge. The data processing, analysis, and visualization were done in R software (R Core Team, 2022).

1.4. Data analysis

The data analysis included three main steps: (1) scaling from probe to whole-tree sap flow, (2) assessing sap flow variability within and between species and (3) understanding the environmental drivers of the observed patterns in sap flow. The scaling procedure followed established literature, and relative biases in whole-tree sap flow were estimated. The intra-species differences in sap flow were investigated within an individual tree and between individuals of the same species along radial (three metrics) and azimuthal (one metric) axes. The inter-specific variability was explored between the two co-occurring functional groups, pioneer species and late-successional species. Species-wise multiple linear regression models were used to understand the drivers of day and night sap flow patterns. SPAC interactions were explored using lag regression analysis while accounting for the relative time lags across the different seasons. The observed temporal lag was combined with a Generalized least squares (GLS) regression time-series model to quantify the relative influence of key environmental drivers, including solar radiation and VPD, on sap flow in the there species.

2.4.1. Scaling from the probe to whole-tree sap flows & bias estimation

2.4.1.1. Scaling from sap flux density to whole-tree sap flow

In trees with radial probes, a combination of the zero-averaged technique and weighted mean method was used to estimate whole-tree sap flow (V_{rad} in kg hr^{-1}) (for details, see Hatton et al. 1990, Pausch et al. 2000).

$$V_{\text{rad.2cm}} = J_{2cm} * A_{\text{total}} * 10^{-3} \quad (2)$$

Sap flow ($V_{rad.2cm}$ in kg hr^{-1}) in the radial trees was also estimated using only the 2nd cm depth probe (J_{2cm}) and total sapwood area (A_{total}), assuming homogenous radial flow for comparison (equation 2). $V_{rad.2cm}$ showed significant overestimation (15 %) in reference to sap flow estimated using radial profile V_{rad}. Previous studies have used simple linear regression models (LRMs) between integrated whole-tree sap flow (V_{rad}) and sap flow in the outer xylem for the trees with only outermost probes ($V_{rad.2cm}$) (Paudel *et al.*, 2013; Berdanier *et al.*, 2016). However, considering the diurnal variability in their relationships, linear regression models without intercept were fitted separately for each hour of the day for each species (Supplementary Table S1). The slopes (m) of the LRMs for each hour were multiplied by the average sap flux density between the north (J_{north}) and the south-facing (J_{south}) probes and the total sapwood area (A_{total}) to estimate sap flow in the replicate trees ($V_{rep.LM}$ in kg hr^{-1}) using equation 3 (Paudel *et al.*, 2013; Berdanier *et al.*, 2016).

$$V_{\text{rep.LM}} = \left(\frac{J_{\text{north}}+J_{\text{south}}}{2}\right) * A_{\text{total}} * m * 10^{-3} \quad (3)$$

2.4.1.2. Biases in the estimation of whole-tree sap flow

The relative biases in V were estimated in replicate trees by systematically ignoring radial and azimuthal variability and compared with whole-tree sap flow estimated by incorporating radial variability ($V_{rep.LM}$, equation 3) as the reference (Shinohara *et al.*, 2013). First, whole-tree sap flow without incorporating the radial variability ($V_{rep.CM}$ in kg hr^{-1}) was estimated by multiplying the total sapwood area (A_{total}) by the average of J at the two diametrically opposite 2-cm probes (equation 4). Second, whole-tree sap flow ignoring azimuthal variability ($V_{rep.N}$ in kg hr^{-1}) was estimated by multiplying only the north-facing probe (J_{north}) and A_{total} (equation 5).

$$V_{rep.CM} = \left(\frac{J_{north}+J_{south}}{2}\right) * A_{total} * 10^{-3} \quad (4)$$

$$V_{rep.N} = J_{north} * A_{total} * 10^{-3} \quad (5)$$

2.4.2. Intra and interspecific variability in sap flow

2.4.2.1. Intra-specific (within a species) variability in sap flow

Within a species, the sap flow variabilities were visualised and quantified as the variabilities in xylem conductivity along the radial and azimuthal profiles. The radial sap flow variability was observed in one tree per species and quantified using three metrics (Delzon *et al.*, 2004; Fiora and Cescatti, 2006):

i. Daily maximum sap flux density (J_{max}) was plotted against the depth from the cambium to indicate regions of high sap flux in the sapwood.
ii. The percentage contribution of sapwood annuli at each depth to daily V was estimated as a product of the sapwood area of the annulus and the corresponding J values.
iii. Hourly correction factors (C_h) were estimated for sunny days in trees with radial probes as the sum of hourly ratios of J at different depths in reference to J_{2cm}, normalized by the sapwood area of the annulus (A_i) over A_{total} (Delzon *et al.*, 2004) (equation 6).

$$C_h = \sum_{i=1}^{n} \left(\frac{J_i}{J_{2cm}}\right) * \left(\frac{A_i}{A_{total}}\right) \quad (6)$$

The azimuthal variability in sap flow was quantified using Sap flow ratios (R_{NS}), estimated as hourly ratios between J_{north} to J_{south}, and the results were averaged for the replicate trees for each species (Shinohara *et al.*, 2013). The coefficients of variability (CV) were estimated for individual trees and averaged for the species for

the key sap flow parameters, sap flux density (J), whole-tree sap flow (V), nocturnal sap flow (V_{Night}), and the Sap flow ratios (R_{NS}) (Wang *et al.*, 2018).

2.4.2.2. Inter-specific (between species) variability in sap flow

Diurnal patterns in the sap flow of the three species were assessed for variability across seasons. The inter-specific variability focused on the relative differences in sap flow along the radial and azimuthal profiles between the three species. Species-wise multiple linear regression models (MLRMs) were fitted for the day (0600-1800 h) and night (1800-0600 hr) periods to assess the relative roles of environmental variables, R_s, VPD, and S, in driving indices of radial (C_h) and azimuthal (R_{NS}) variability (Moore *et al.*, 2011; Barbeta *et al.*, 2012). C_h values above and below one suggest underestimation and overestimation by the 2nd cm probe in reference to the rest of the xylem, respectively. Similarly, R_{NS} values above one suggests dominant flow was on the north-facing part of the trunk, while R_{NS} below one suggests the dominance of the south-facing part of the trunk. Sap flow between 1800-0600 hr was considered nocturnal (V_{night}), and its percentage contribution to daily V was estimated. V_{night} was further split into the evening (1800-0000 hr, $V_{evening}$) and pre-dawn (0000-0600 hr, $V_{pre-dawn}$) components (Forster, 2014). Species-wise MLRMs, using V_{night} as the response variable and VPD, S, and wind speed (u) as predictor variables, were fitted to quantify the environmental drivers of nocturnal sap flow (Barbeta *et al.*, 2012). In the MLRMs, R_s, VPD, u, and S were normalized by their respective daily means to facilitate the interpretation of the results.

2.4.3. Environmental controls on sap flow under SPAC

2.4.3.1. Lag analysis between sap flow and SPAC variables

Exploratory linear regression models yielded poor results for interactions between sap flow and environmental drivers, which were temporally lagged due to phase differences (Bond *et al.*, 2002). Thus, lag correlation analysis was used to compute seasonal changes in the time lag between the environmental drivers and whole-tree sap flow (V) (Moore *et al.*, 2011). The S time-series was de-trended to extract the diurnal signals (S_{diu}) (*stlplus* function, package *stlplus* in R). Hourly lag was computed (*ccf* function, package *stats* in R) for each day between R_s *vs* V, VPD *vs* V, and S_{diu} *vs* V, at the tree-level for the three species. The days with significant auto-correlation coefficients (ACF >= |±0.4|) were plotted for the three species. Positive

autocorrelation coefficient (ACF) values signified that a high value of the driver variable was followed by a high value of the response variable after the corresponding lag hours. In contrast, a negative ACF value denoted that a high value of the driver variable was followed by a low value of the response variable. Similarly, positive lag hours indicated that the driver variable led the response variable and negative lag hours indicated that the driver variable lagged behind the response variable.

2.4.3.2. GLS linear regression model for whole-tree sap flow

The relative influences of environmental (predictor) variables on the whole-tree sap flow (response) variable were quantified using a combination of a temporal lag and Generalized least squares (GLS) regression models (*gls* function, package *nlme*) with a suitable correlational structure. The GLS regression method estimates the maximum likelihood of the regression coefficients using generalized least-squares and is suitable for analyzing time-series data with auto-correlational structures (Pinheiro and Bates, 2006; Krishnaswamy *et al.*, 2012). The GLS model used R_s, VPD, and S as predictor variables, which were normalised by subtracting the daily mean from the time-series, and checked for collinearity. The second-order autoregressive moving average (corARMA) was found to be the best fit correlational structure. The GLS model with corARMA structure was run separately for each tree to capture the interactions at intra-species and interspecific levels. Contiguous subsets longer than five days without missing values were tested for the time lag between the driver and response variables (*ccf* function in R). If any significant lag (ACF >= |±0.4|) was observed, the driver variable was lagged by a suitable range of hours to develop a multiple-lagged time-series starting from zero lag time and a linear regression model was fitted with the response variable. The procedure was repeated for each of the driver variables, and the lagged time-series with the lowest lag hours (P =< 0.05) was chosen to develop a reconstituted dataset. The GLS model with corARMA structure was compared against a similar GLS model without any autocorrelation structure using the Analysis of variance (ANOVA) test. The GLS model with the lowest Akaike information criterion (AIC), higher likelihood ratio, and significance was chosen for interpretations. The model performance was assessed using a linear regression model, and Kling-Gupta Efficiency (KGE) score for the observed and predicted V (Gupta and Kling, 2011).

Results

3.1. Intraspecific variability in sap flow

3.1.1. Radial variability in sap flow

Radial patterns in J_{max} varied considerably across the three species. Both *S. racemosa* and *E. acuminata* exhibited concave curves in J_{max}, with comparable peaks at the outer (37.4±15 cm^3 cm^2 hr^{-1}) and innermost (41.3±23 cm^3 cm^2 hr^{-1}) xylem (Figure 1A). Correspondingly, the percentage contribution of each depth to daily V declined uniformly from the outermost xylem inwards for *S. racemosa* and *E. acuminata* (Figure 1B). Conversely, *C. hystrix* showed the peak J_{max} (23.1±14 cm^3 cm^2 hr^{-1}) at the inner xylem (4^{th} cm depth from the cambium) and its contribution to daily V was disproportionately higher (40 %) than the rest of the depths. Following the above pattern, the highest wood moisture and lowest wood density were also observed at the 1^{st} cm depth in *S. racemosa* and *E. acuminata*, and at the 4^{th} cm depth in *C. hystrix* (Supplementary Figure S3). Overall, mean hourly J increased with wood moisture and declined with wood density for a particular sapwood annulus ring, except for *E. acuminata* (Supplementary Figure S4). The relative contributions of sapwood annuli to whole-tree sap flow remained similar for both day and night periods and across the species. The innermost probe (5^{th} cm depth) in *C. hystrix* stopped showing sap flux movement after January, indicating the loss of conductivity in the annuli as the inner sapwood transitioned into non-functioning heartwood (Brodersen *et al.*, 2019).

Figure 1. Radial variability in sap flow in the three species along the depth of xylem in (A) average daily maximum sap flux density (J_{max}, cm^3 cm^2 hr^{-1}) and (B) percentage contribution of sap flow at different sapwood depths to daily whole-tree sap flow (V, kg hr^{-1}) (the error bars represent standard errors).

The three species displayed contrasting diurnal patterns in the radial correction factor (C_h) (Supplementary Figure S5A). In *S. racemosa* and *E. acuminata*, the 2^{nd} cm probe underestimated sap flow in reference to the rest of the xylem (C_h >1) in the evening-night period (1700-0400 h) and overestimated (C_h < 1) in the day (0400-1700 h). Contrastingly, in *C. hystrix*, the 2^{nd} cm probe overestimated sap flow (C_h > 1) in night-morning (2300-0900 h) and overestimated (C_h < 1) in noon-evening (1000-2200 h) periods. On a closer look, the variability in C_h was driven by the higher sap flux density at the outer xylem (1^{st} cm depth) in *S. racemosa*

and *E. acuminata*, and at the inner xylem (4th cm depth) in *C. hystrix* to the rest of the xylem. The MLRMs results suggested that daytime radial variability (C_h) was strongly predicted by R_s (negative slope) and S (positive slope) in *S. racemosa* ($r^2 = 0.43$, $P < 0.001$), whereas none of the predictors was significant for *E. acuminata* ($r^2 = 0.01$, $P < 0.6$) and *C. hystrix* ($r^2 = 0.01$, $P < 0.15$) (Supplementary Table S2). Conversely, VPD was a strong negative predictor of night C_h in *E. acuminata* ($r^2 = 0.4$, $P < 0.001$), but not in *S. racemosa* ($r^2 = 0.02$, $P < 0.2$) and *C. hystrix* ($r^2 = 0.001$, $P < 0.6$).

Both *S. racemosa* and *E. acuminata* exhibited consistently high azimuthal sap flow ratios (R_{NS}) throughout the day (Supplementary Figure S5B). Interestingly, in *C. hystrix*, the northern probes dominated in the morning, with large standard deviations, suggesting significant intra-specific variability. The southern probes peaked from the afternoon onwards in *C. hystrix*. The MLRMs predicting R_{NS} performed poorly ($r^2 \sim 0.03$-0.18) across the species (Supplementary Table S3). However, R_s (positive slope) was a significant predictor of R_{NS} at moderate values of VPD and S across the three species ($P < 0.09$). Night-time azimuthal variability was better predicted by VPD ($P < 0.06$) and S ($P < 0.08$) in *S. racemosa*; and by VPD in *C. hystrix* ($P < 0.004$). S was a significant predictor of night R_{NS} in *E. acuminata* ($P < 0.04$).

3.1.2. Sap flow variability between individuals of the same species

The CV between the three species was very high in all sap flow parameters, J (255 %), V (246 %), V_{Night} (147 %), and R_{NS} (236 %). The CV in J was significantly higher among individuals of *S. racemosa* (282±32 %) and *E. acuminata* (267±30 %) than *C. hystrix* (179±12 %) (Table 3). Similarly, the CV in V was significantly higher between individuals of *S. racemosa* (279±49 %) and *E. acuminata* (273±22 %) than *C. hystrix* (170±5 %). The intra-specific variability in nocturnal sap flow was almost double in the pioneer species, *S. racemosa* (155±32 %) and *E. acuminata* (140±34 %), then *C. hystrix* (78±3 %). Conversely, the CV in azimuthal variability was almost double in *C. hystrix* (273±28 %) than in *S. racemosa* (114±56 %) and *E. acuminata* (96±60 %).

Table 3. Estimates of sap flux density (J, $cm^3\ cm^2\ hr^{-1}$), whole-tree sap flow (V, $kg\ hr^{-1}$), tree-to-tree coefficient of variation in sap flow (CV) and percentage biases in sap flow estimation due to ignoring radial and azimuthal variability (standard deviation in parentheses) in the studied species.

3.2. Interspecific variability in sap flow and environmental drivers

3.2.1. Comparisons of sap flux density and whole-tree sap flow

The pioneer species, *S. racemosa* and *E. acuminata*, exhibited double rates of sap flux density (J) and whole-tree sap flow (V) in comparison to *C. hystrix*, the late-successional species (Table 3). The whole-tree sap flow (V) was linearly related to the total sapwood area ($r^2 > 0.71$, $P < 0.001$). The larger girth size in *C. hystrix* was offset by a significant proportion of non-conducting heartwood, whereas the pioneer species *S. racemosa* and *E. acuminata* showed a significantly higher proportion of conducting sapwood contributing to high V rates. Radial bias, due to assumptions of homogenous flow along the xylem, led to overestimations of V in the three species. The failure to account for azimuthal variability (azimuthal bias) caused a significant underestimation of V in *S. racemosa* and *C. hystrix* but overestimated in *E. acuminata*.

3.2.2. Diurnal patterns in sap flow in relation to environmental drivers

The peak sap flow in *S. racemosa* and *E. acuminata* occurred relatively early in the day (0700-0800 h), whereas *C. hystrix* peaked around noon (1200 h) (Figure 2). Both *S. racemosa* and *E. acuminata* showed low sap flow at high values of R_s and VPD (Supplementary Figure S6). The heightened sensitivity to the environmental extremes manifested in bimodal peaks in diurnal sap flow with significant midday depression (V_{midday}) across the sampled trees. The timing of V_{midday} coincided with peaks in VPD and R_s and troughs in S. Contrarily, *C. hystrix* maintained high V at extreme R_s and VPD with a unimodal peak, although minor signs of V_{midday} were seen in two of the three trees.

Figure 2. Diurnal patterns of sap flow (V, kg hr^{-1}), Incoming short-wave radiation (R_s, kW m^{-2}), and Vapour pressure deficit (VPD, kPa) across the three species (values are normalized by their respective daily means for visual scaling and error bars represent standard errors).

3.2.3. Nocturnal sap flow

Nocturnal sap flow (V_{night}), as a fraction of daily V, was highest in *E. acuminata* (17.2±9 %), followed by *C. hystrix* (13.5±5 %) and *S. racemosa* (11.3±7 %) (Table 4). A significant proportion of V_{night} occurred at pre-dawn in *S. racemosa* (6.2±7 %), whereas evening flux dominated in *C. hystrix* (9.7±5 %). The proportion of evening-night (9.5±8 %) was marginally higher than pre-dawn (7.7±7 %) sap flux in *E. acuminata*. At night, the environmental conditions fluctuated between high wind and high VPD to relatively quieter periods with low VPD. Across the species, the high values of V_{night} were associated with low VPD (< 0.1 kPa), low wind velocity (< 0.5 m s^{-1}), and moderately saturated soil moisture conditions (Supplementary Figure S7). The MLR models predicting V_{night} concurred with the observations of VPD, soil moisture and wind acting as limiting variables to nocturnal sap flux (Supplementary Table S4). S (negative slope) was a significant predictor of V_{night} in *E. acuminata* (r^2 = 0.12, P < 0.05) and VPD (negative slope) was a significant predictor for *C. hystrix* (r^2 = 0.13, P < 0.009). None of the predictors were significant for *S. racemosa* (r^2 = 0.02, P > 0.5).

Table 4. Percentage contribution of day, night, evening and pre-dawn sap flow to total daily sap flow in the three species (values in %, the standard deviation in parentheses).

3.2.4. Seasonal changes in diurnal patterns of sap flow, transpiration, and environment

Figure 3 depicts changes in diurnal patterns of SPAC variables from winter to summer as the growing season progressed. The winter (December-February) marked the dry season with sunny but cold days, sub-zero night temperatures, low VPD, and declining soil moisture. In March, rains replenished the soil moisture reserves and promoted leaf flush. The summers (March-May) saw increased day length (Figure 3A), abundant moisture, warmer temperatures, and higher VPD (Figure 3B). Consequently, V also increased from winter to summer, peaking in April, but with considerable variation in the three species. Both *S. racemosa* and *E. acuminata* exhibited peak sap flow in December and March, whereas *C. hystrix* peaked in March-April (Figure 3D, 3E and 3F). The intra-specific variability in sap flow also followed similar patterns. Radial variability in sap flux (C_h) increased in the dry season for *S. racemosa* and *E. acuminata*, whereas *C. hystrix* exhibited the highest variability in March and April (Supplementary Figure S8). The fractional contribution of the outer xylem to

daily V increased from December to March for *E. acuminata* and *C. hystrix*, whereas the corresponding changes were marginal in *S. racemosa* (Supplementary Figure S9). Sap flow ratios (R_{NS}), the metric for azimuthal variability, also increased from winter to summer for *S. racemosa*, whereas in *C. hystrix* it was highest in January. Diurnally, the peak sap flow values increased with the growing season, except for *S. racemosa*, although the timing of peak V remained consistent across the species. The bimodal peaks in diurnal sap flow were seasonally consistent for *S. racemosa* and *E. acuminata*, with higher rates in the morning than afternoon. In dry winter, the relatively milder $V_{mid\text{-}day}$ behaviour was observed in two out of three trees of *C. hystrix*, which shifted to unimodal peaks from March onwards. In the three species, weak declining trends in V_{night} were observed from the dry to the wet season. The diurnal peaks in S_{diu} shifted from afternoon to evening with increasing amplitude from winter to summer (Figure 3C).

Figure 3. Seasonal changes in diurnal patterns of SPAC variables from winter (December) to summer (May): (A) Incoming short-wave radiation (R_s), (B) Vapour Pressure Deficit (VPD), (C) S_{diu} is the diurnal component of soil moisture, (D), (E) and (F) are the whole-tree sap flow rates (V) of *S. racemosa*, *E. acuminata*, and *C. hystrix*, respectively. Each line represents monthly average values.

3.3. Environmental controls on transpiration under SPAC

3.3.1. Lag analysis between transpiration and SPAC variables

V consistently lagged behind R_s in all three species by an average lag of 1-3 hr and strong positive correlations in winter and summer, with the lowest variability in *C. hystrix* (Figure 4). However, in *S. racemosa* and *E. acuminata*, VPD lagged V in winter and led V in summer with positive correlations. VPD led V across seasons in *C. hystrix*. On closer scrutiny, the days when V preceded R_s and VPD with strong positive correlations were marked by significant pre-dawn flux, and the frequency of such days was significantly higher in *S. racemosa* and during the dry winter (January and February). However, the interactions between V and S_{diu} were more complicated. On most days in winter (75 % of total days), V led S_{diu} with a 1-3 hr lag and positive correlations, while on the remaining days, V lagged behind S_{diu} by 1-5 hr and negative correlations in the three species. However, the patterns reversed from March onwards with the advent of rains, S_{diu} led V by 1-3 hr and negative correlations in the three species on the majority of the days (77 % of total days), while on the

remaining days, S_{diu} lagged behind V by 1-5 hr and positive correlation. The lag between transpiration and soil moisture was also positively correlated to tree size, i.e., the larger-sized trees (>0.15 m DBH) experienced lesser lag between transpiration and soil moisture in winters in *S. racemosa* and *E. acuminata*, and in summers in *C. hystrix*, but the results were not significant.

Figure 4. Boxplots showing seasonal shifts in daily lag hours at maximum auto-correlation coefficients (ACF) between SPAC variables in individual trees of the three species: Incoming short-wave radiation (Rs, kW m^{-2}), Vapour pressure deficit (VPD, kPa), whole-tree sap flow (V, kg hr^{-1}) of *S. racemosa*, *E. acuminata* and *C. hystrix* and the diurnal component of soil moisture (S_{diu}, mm). The horizontal dotted line marks zero lag hours. The colour of the boxplot represents the direction of the ACF values, and the values around the boxplots are the number of data days.

3.3.2. GLS linear regression model for whole-tree sap flow

The sap flow modelling exercise was carried out for five (8±2 days), four (10±5 days) and ten (10±4 days) contiguous data periods (without missing values) across winter and summer for the instrumented trees of *S. racemosa*, *E. acuminata*, and *C. hystrix*, respectively (Table 5). The GLS model with corARMA structure had significantly lower AIC than the GLS model without any correlational structure. In summer, VPD (positive slope) emerged as a significant predictor of whole-tree sap flow (V) at average values of R_s and soil moisture for the three species. In winter, the R_s was a co-driver of V for *E. acuminata*, and *C. hystrix* with positive coefficients, while S was a significant predictor of V in one of the trees of *C. hystrix* with a positive coefficient. Interestingly, one tree per species showed negative R_s coefficients in winter and summer, respectively, albeit with low significance (P>0.1), indicating the occasionally limiting role played by R_s. S was not a significant predictor of V. However, it is important to note that soil moisture always remained well above the permanent wilting point of the site. The relative strength of interactions between V and environmental drivers varied between individual trees of the same species and across the seasons.

Table 5. Results from Generalized least squares (GLS) linear regression model with corARMA structure for whole-tree sap flow in the trees of *S. racemosa*, *E. acuminata* and *C. hystrix* (*P < 0.05, ** P < 0.01, *** P <

0.001). Predictor variables include Incoming short-wave radiation (R_s, kW m^{-2}), Vapour Pressure Deficit (VPD, kPa), whole-tree sap flow (V, kg hr^{-1}) and soil moisture (S, mm).

In *S. racemosa*, VPD was the only significant predictor of V in all the trees. In *E. acuminata*, VPD was the sole significant predictor of V in one of the trees in summer, while in another, VPD and R_s were significant co-predictors in winter. In *C. hystrix*, both VPD and R_s were significant predictors with positive coefficients in six out of ten periods across seasons, except for one period in Tree 3 in summer, where R_s showed a negative coefficient. The GLS model performed relatively better for *S. racemosa* (r^2 = 0.15, P < 0.001, KGE = 0.12) than *E. acuminata* (r^2 = 0.08, P < 0.001, KGE = 0.02) with improved concurrence between predicted and observed V. In both species, the predicted V failed to replicate the bi-modal patterns in the observed V and underestimated overall sap flow (Supplementary Figure 10A and 10B). However, the model performance was significantly improved for *C. hystrix* (r^2 = 0.41, P < 0.001, KGE = 0.43), with the predicted V matching well with the unimodal patterns and sap flow volumes (Supplementary Figure 10C). However, the predicted V had synthetic sap flow in the night hours for the three species, which was absent in the observed V.

Discussion

4.1. Influence of secondary forest structure on sap flow variability in co-occurring species

The root-trunk-leaf connectivity in the xylem is a fascinating area of research under SPAC, largely dominated by the century-old cohesion-tension theory and piped model of water transport (Kim *et al.*, 2014). The unit-pipe model postulates direct connections between root and lateral branches (known as sectoral flow) and is a common feature of ring-porous species. Conversely, diffuse-porous species exhibit considerable lateral connectivity (known as integrated flow), where multiple parts of the crown are supported by a cross-section of the xylem. Interestingly, pruning experiments show that, within the same individual, the outer xylem can exhibit sectoral connectivity, while the inner xylem may show an integrated flow pattern (Čermák and Nadezhdina, 2011; Dong *et al.*, 2019). In this study, the observed Gaussian radial profile with increasing sap flux density in the inner xylem in *C. hystrix*, a ring-porous species, suggests sectoral connectivity, which is also typical of isolated trees with an extended crown (Fiora and Cescatti, 2006). The Gaussian radial profile is ascribed to higher light availability to the older portions of the crown around the periphery, which are anatomically

connected to the inner xylem. Conversely, in trees forming a continuous canopy, like *S. racemosa* and *E. acuminata* (both diffuse-porous species) at the study site, the lateral foliage activity is suppressed by shading, and only the top portion of the crown receives proper light, inducing higher sap flux density in the outer xylem. It was supported by the observed overestimation of radial correction factors ($C_h < 1$) in the outer xylem of in-canopy pioneer species, *S. racemosa* and *E. acuminata*, and underestimation by ($C_h > 1$) in the outer xylem in late-successional emergent trees of *C. hystrix*. Delzon et al. (2004) observed that the radial correction factors were independent of meteorological factors and better represented the xylem-crown-water-use connectivity.

Further, in sloped terrains, landscape characteristics like slope and aspect influence the diurnal changes in the angle and intensity of incident light, potentially inducing azimuthal variability in sap flow (Kumagai *et al.*, 2007; Berry *et al.*, 2016). Research shows higher connectivity between lateral branches (and leaves) and fine root development on the same aspect of trees (Čermák and Nadezhdina, 2011; Dong *et al.*, 2019). Along the same line, we observe that fully exposed crowns of *C. hystrix* exhibited shifting peaks in sap flow from north to south-facing xylem following the NE-SW trajectory of sunlight, whereas the in-canopy, *S. racemosa* and *E. acuminata*, maintained dominant sap flow at the northern probes. Interestingly, the CV in azimuthal variability was almost double in emergent trees of *C. hystrix* than in the in-canopy pioneer species *S. racemosa* and *E. acuminata*. Daytime radial and azimuthal variability in the three species was attributed to the interaction between access to solar radiation and soil moisture, whereas nighttime variability was negatively correlated with VPD (Fiora and Cescatti, 2006; Shinohara *et al.*, 2013). The biases in estimating V due to ignoring azimuthal and radial variability were significant and comparable to existing literature (Fiora and Cescatti, 2006; Shinohara *et al.*, 2013).

4.2. Differential water-use strategies among pioneers and late-successional species

Functional groups play a major role in driving interspecific variability in transpiration (Nogueira *et al.*, 2004; Motzer *et al.*, 2005). Our observations of high J in pioneer species, *S. racemosa* and *E. acuminata*, align well with the observations from co-occurring tree species in semi-arid China, which show high transpiration rates by pioneer species, especially in the growing season (Lyu *et al.*, 2020) and from wet Brazilian rain forests, where Nogueira et al. (2004) report pioneer species showing higher intrinsic water use efficiency (the ratio of net photosynthetic CO_2 assimilation to stomatal conductance) and instantaneous transpiration efficiency (ratio of photosynthesis rate to transpiration) than late-successional species, while maintaining high sap flux rates.

Similarly, studies report higher leaf-level hydraulic conductance and photosynthetic capacity in pioneer species than in late-successional species from South American TMF (Sobrado, 2003; dos Santos *et al.*, 2019) and Central Panama (Bretfeld *et al.*, 2018).

Like true pioneers, *S. racemosa* and *E. acuminata* are the first tree species to occupy any disturbance-related openings, but they also occur as sub-canopy associates to late-successional Fagaceae species in old-growth TMFs in Sikkim, indicating long-term recruitment of pioneer species. Expanding the conventional segregation of species along the fast-slow/growth-survival axes, Rüger *et al.* (2020) suggest a third axis of stature-recruitment trade-offs distinguishing long-lived pioneers (fast-growing, live longer, attain tall canopy stature but low recruitment) from short-lived breeders (fast-growing, short-statured, low survival but a high number of offspring). In a meta-analysis of over 5000 species across 13 long-term monitoring plots, Kambach *et al.* (2022) show that fast-slow continuum and stature-recruitment are independent life-history strategies shaping tropical secondary forests globally. Although long-term studies are lacking from the landscape, *S. racemosa* and *E. acuminata* can be characterized as long-lived pioneers (LLPs) owing to their ability to grow fast during the initial period after disturbance but also to be able to adapt and live longer as the forest matures. LLPs are critical secondary forest species and dominate the intermediate successional stages in terms of carbon sequestration and water-use (Rüger *et al.*, 2020; Lai *et al.*, 2021).

The pioneer species, *S. racemosa* and *E. acuminata*, also displayed increased radial and azimuthal variability in summers and consistent midday depression, an indicator of efficient stomatal control over plant-water use. The GLS modelling results showed that at least one tree from each of the three species displayed the limiting effect of solar radiation (R_s) on V (negative coefficients). The heightened sensitivity to environmental extremes in the pioneer species is attributed to their canopy position, which exposes them to strong levels of sunlight and VPD causing midday stomatal closure (Huc *et al.*, 1994; Franco and Lüttge, 2002; Chiariello *et al.*, 2006). It is also attributable to their shallow rootedness and sensitivity to diurnal and seasonal soil moisture fluctuations (Pavlis and Jeník, 2000), although observed topsoil moisture (0-30 cm depth) never went below the permanent wilting point. In a relevant study, Bretfeld *et al.* (2018) quantified the impact of El Niño-induced drought years on sap flow in 76 species across different successional stages (8-80-year-old forests) in Central Panama. They observed that the limiting role of seasonal soil moisture stress is stronger in pioneer species than in late-successional species. Similar reports from Central Himalayan species belonging to Fagaceae family, such as *Castanopsis indica*, *Quercus semicarpifolia*, *Quercus leucotrichophora*, and sub-canopy *Rhododendron*

arboreum, show that seasonal soil moisture stress can induce midday slump in leaf-water potential (Zobel *et al.*, 2001; Poudyal *et al.*, 2004; Tewari *et al.*, 2018). The absence of significant midday depression in deep-rooted species like *C. hystrix* at the peak of the dry season and strong diurnal cycles in soil moisture provide evidence of vegetation accessing moisture from deeper soil layers (Kumar *et al.*, 2022 Preprint; Tanaka *et al.*, 2004; Allen, 2014).

Our observations of 2-3 h of lag between R_s and VPD and V were seasonally consistent and comparable with reports from TMFs in Costa Rica (Moore *et al.*, 2018) and marginally higher than reports from Tibet (~1-hour lag) (Wang *et al.*, 2017). Since these are stem-based measurements, the lags could be confounded by delays between stem sap flow and canopy transpiration due to hydraulic capacitance and resistance, although such lag is usually <= 1 hour (Phillips *et al.*, 1997; Burgess and Dawson, 2008). The longer lags (>1 hour) observed may also represent delays induced by low morning temperatures in winter and leaf wetness in the summer due to night rains or dew (Aparecido *et al.*, 2016; Bretfeld *et al.*, 2018; Moore *et al.*, 2018). Although rains in summer usually start at noon, a significant part also fell in the pre-dawn period (Kumar *et al.*, 2021). Thus, incorporating leaf wetness as a variable is recommended for future studies from wet TMFs like Eastern Himalaya, which experiences significant summer rains.

4.3. Plant-water relations in wet and high-elevation Eastern Himalayan TMFs

4.3.1. High sap flow rates in wet TMF climatology

The observed J in the three species was significantly higher than their respective conspecifics from other TMFs. The observed J in *C. hystrix* at our site was three times higher than conspecific *Castanopsis tribuloides* from relatively drier (MAP = 1331 mm) Central Himalaya (Ghimire *et al.*, 2014). Similarly, The observed J for *Symplocos racemosa* and *Eurya acuminata* were 6-9 times higher than conspecifics from drier environments: *Symplocos ramosissma* in China (MAP ~2000 mm) and *Symplocos kuroki* and *Eurya japonica* in Japan (MAP ~1700 mm), respectively (Chiu *et al.*, 2016; Zhang *et al.*, 2018). The observations of higher sap flux density and sap flow in pioneer species (*S. racemosa* and *E. acuminata*) than late-successional species (*C. hystrix*) have been previously reported from tropical lowland secondary forests of Costa Rica (40 masl), and high-elevation TMFs from Panama (1800 masl) and Ecuadorian Andes (~2000 masl), and commonly attributed to higher water movement potential of pioneer species (Motzer *et al.*, 2005; McCulloh *et al.*, 2011). The

potential role of soil mycorrhizae and root hair densities in facilitating the high transpiration rates observed in these forests is another recommended area for future research (Carminati *et al.*, 2017).

4.3.2. Nocturnal sap flow in Himalayan tree species

The nocturnal sap flow observed is one of the first records for the pioneer species *S. racemosa* and *E. acuminata* globally and *C. hystrix* from TMFs. For *C. hystrix*, the previous reports from higher latitudes in China are significantly lower (4 %) than our observations (Chen *et al.*, 2018; Wang *et al.*, 2018). Contrary to reports by Wang et al. (2018), the observed intra-specific variability in nocturnal sap flow was lesser than the inter-specific variation in *C. hystrix*. However, concurring with Kangur *et al.* (2021), higher intra-specific variability in nocturnal sap flow was seen in the pioneer species, *S. racemosa* and *E. acuminata*, indicative of a broader range of responses to similar environmental stressors. According to the literature, the ecophysiological mechanism driving nocturnal sap flux can be broadly categorized into (A) Refilling of the stem, (B) facilitating night respiration, and (C) endogenous stomatal controls. In this study, the bulk of the nocturnal sap flux occurred in the evening and is attributed to the capacitive refilling of the stem (Wang *et al.*, 2018; Kamakura *et al.*, 2021). In similar reports from broadleaved evergreen species in East Asia, nocturnal sap flux is attributed to stem recharge and shows low correlations with environmental variables like VPD (Chen *et al.*, 2018; Wang *et al.*, 2018; Zhang *et al.*, 2020). Nocturnal movement of water to restore hydraulic equilibrium between root-shoot-leaf is a known feature of large trees, although not restricted to them, and in the study, both evening and pre-dawn sap flux were independent of tree size (Zeppel *et al.*, 2011; Siddiq and Cao, 2018).

Interestingly, Chen et al. (2018) also report significantly higher nocturnal sap flux in tree species with corticular photosynthetic capacity (*C. hystrix* being one of the common study species), indicating a role in facilitating respiration. Chen et al. (2018) also highlight the role of nocturnal sap flux in oxygen transport to the internal xylem during nocturnal respiration, a possible mechanism to alleviate hypoxia-like conditions created in internal photosynthesising xylem tissue during respiration. Further, Marks and Lechowicz (2007) show that nocturnal sap flux is closely linked to leaf nitrogen concentrations and higher rates of extension growth in fast-growing shade-intolerant pioneer species and attributed it to night-time respiration, which facilitates carbohydrate translocation and other processes associated with the growth of meristems in roots and shoots. Lastly, the role of endogenous (circadian-driven) stomatal control in regulating nocturnal sap flux under stable VPD, low wind and moderate soil moisture conditions merits further investigations (Resco de Dios *et al.*, 2013;

De Dios *et al.*, 2015). Under an experimental setup, Chu et al. (2009) demonstrated a significant positive correlation between wind speed and nocturnal sap flux up to a threshold when stomatal closure is assumed to limit transpiration. Similar to our observations, in a garden experiment involving temperate broadleaved species, Kangur *et al.* (2021) found significant nocturnal (pre-dawn) stomatal conductance in the anisohydric pioneer species in comparison to the isohydric late-successional under hydrated conditions and attributed it to contrasting life-history traits dictating stomatal controls. Kumar et al. (2021) observe a significant diurnal cycle in summer precipitation, starting from noon and leaving a short 5-6 hr window conducive to plant productivity and transpiration. Pre-dawn flux is an uncommon observation from the Himalaya and, as Barbeta et al. (2012) observed in the Mediterranean, could potentially be an adaptation to ensure hydraulic saturation in the stem, avoid leaf-level moisture leakage, and maximise photosynthetic CO_2 uptake at the start of the day. The prevalence of the phenomenon across both pioneer and primary tree species suggests that traits might indeed be conserved as an adaptation and merit further investigations (Kangur *et al.*, 2021).

4.4. Energy vs. Moisture limitations on sap flow in Eastern Himalaya

The study site experienced strong seasonal fluctuations in energy and temperature with moisture and energy-limited winters. The resultant seasonal variability in the interactive roles of sunlight and VPD as drivers of sap flow have been previously reported from TMFs (Moore *et al.*, 2018). It was observed that VPD was a stronger driver of sap flow than R_s and S in both summer and winter, independent of functional groups, which is in concordance with reports from Central Himalaya (Ghimire *et al.*, 2014) and Central Panama (Bretfeld *et al.*, 2018). However, during periods of sufficient soil moisture but limited energy availability in winter, sap flow was also driven by R_s, similar to observations from TMF in Southern Andes (Motzer *et al.*, 2010) and the Alps (Fiora and Cescatti, 2006). As discussed earlier, we also found evidence of photosensitivity in the study species through the inhibitive impact of R_s on sap flow, similar to reports from Brazilian TMFs (dos Santos *et al.*, 2019). Soil moisture was both a limiting variable for pioneer species, as seen with the positive lags and negative autocorrelation coefficients, and a stock depleted by vegetation water use, especially by the deep-rooted and large-sized individuals of Fagaceae (late-successional species) (Kumar *et al.*, 2022 Preprint). The results correspond to similar observations from Central Panama where older and large-sized late-successional species kept transpiring unfazed even under drought conditions, while younger pioneer species reduced their water-use (Bretfeld *et al.*, 2018). Here, the role of sapwood area (as a parameter of conducting capacity of the tree) and

tree size (representing the age and form of the tree) on the ability of different species to withdraw water from different soil layers and possibly groundwater, becomes of greater interest. The linear increase in whole-tree sap flow with sapwood area is likely to plateau for mature individuals, even under saturated soil moisture conditions, due to limits imposed by stomatal conductance (Gao *et al.*, 2015).

Our observations provide empirical evidence to the theory that the East Himalayan forests are energy-limited under abundant moisture conditions (Sebastian *et al.*, 2019), although VPD remains the primary driver of sap flow independent of successional stages, and soil moisture played a limiting role for pioneer species only (Bretfeld *et al.*, 2018). Under such conditions, along with VPD, solar radiation could be a significant driver of non-monsoon vegetation activity, as observed by Sebastian et al. (2019) using remotely-sensed enhanced vegetation index (EVI) as a proxy of vegetation productivity. The role of solar radiation is further accentuated in uneven-aged secondary forests in the Himalaya, where the social positioning of the trees in the canopy determines the spatial availability of solar radiation to different parts of the crown (Fiora and Cescatti, 2006; Küppers *et al.*, 2008; Zhang *et al.*, 2019). The GLS regression model performance was affected by the inherent variability in sap flow, with complex phenomena like mid-day depression and pre-dawn sap flux dominating the diurnal movements of the pioneer species at the site.

4.5. Changing water availability and implications on carbon sequestration in Himalayan TMFs

Climate change studies from Eastern Himalaya have highlighted an increase in mean annual temperature of 0.02°C yr^{-1} with an estimate of daily average temperature increase by 1.8-4 °C by the end of the 21st Century and increased precipitation by 30-40 % (Singh *et al.*, 2011; Shrestha *et al.*, 2012). Kulkarni et al. (2013) used a high-resolution PRECIS model to project an increase in temperature (up to +5 °C) and precipitation (+40 %) by the year 2098 in Eastern Himalaya. In line with the regional trends, Dimri et al. (2018) used Asian Precipitation-Highly Resolved Observational Data Integration Towards Evaluation of Water Resources (APHRODITE), a gauge-interpolated gridded precipitation product, to observe increasing trends in pre-monsoonal (March-May) and monsoonal (June-September) precipitation in Sikkim Himalaya for 1970-2005. Sharma and Goyal (2020) used four global circulation models and IMD 0.25° gridded precipitation dataset to project 0.4-1.1 °C and 0.5-1.7 °C rise in maximum daily temperature and 220-380 mm and 150-760 mm increases in mean annual precipitation under Representative Concentration Pathway (RCP) 4.5 and RCP 8.5, respectively for our study region for 2011-2100 (covered under SB6 basin in referenced paper). The projected rise in temperature is likely to increase

in both day and night-time VPD leading to higher sap flow rates, which we observe to be among the highest from the tropical montane or lowland forests. The high sap flow rates may get further fueled by the predicted increase in summer and monsoon precipitation (Mcvicar *et al.*, 2010). In winters, the reduced precipitation (low moisture availability) and increased warming (high VPD) may create seasonal drought conditions and induce water stress, especially among pioneer species.

The pioneer species are reported to have higher photosynthetic plasticity and leaf hydraulic conductivity permitting high sap flux rates, while also being vulnerable to xylem embolism due to lower control over water use (Sobrado, 2003; Nogueira *et al.*, 2004; dos Santos *et al.*, 2019). Conversely, despite low photosynthetic plasticity and lower hydraulic conductance, late-successional species are seemingly unfazed by seasonal drought conditions in winter due to better water-use control through stomatal closure and access to deeper subsurface moisture reserves (Sobrado, 2003; Tanaka *et al.*, 2004; Allen, 2014). Additionally, higher VPD is also likely to negatively impact nocturnal transpiration, which might affect the ability of these tree species to utilise the available moisture efficiently. However, the net effect could be easily offset by the potential increase in daytime transpiration. The potential increase in annual net transpiration will most likely change the water balance by negatively impacting soil moisture and hydrological flows from these temperate broad-leaved forests in summers and to a lesser degree in winters.

The impact of the projected increase in atmospheric CO_2 and associated fertilization effect, increase in temperature and precipitation changes on carbon assimilation rates would vary between species groups. The pioneer species are likely to maintain high photosynthesis rates by optimizing leaf-specific conductivity, which is the relationship between conducting area and the leaf area (Sobrado, 2003). Interestingly, Eckert et al. (2021) show that late-successional species have the highest rate of respiratory CO_2 refixation owing to relatively higher mesophyll resistance and thicker cell walls, which allows them to fix more CO_2 while opening fewer stomata and losing less water. Irrespective of the species groups, the CO_2 fertilization effect could induce lesser moisture uptake as the same amount of carbon can be fixed with a lesser number of stomata open or in lesser time (Mengis *et al.*, 2015; Yang *et al.*, 2016; Hashimoto *et al.*, 2019). However, the gain in water-use efficiency with CO_2 fertilization could be offset by higher nocturnal transpiration in secondary forests (Marks and Lechowicz, 2007). Further, the CO_2 fertilization effect could be limited by the availability of soil nutrients, especially nitrogen and phosphorus, in poorly-developed and highly leached mountain soils, such as at our site (dos Santos *et al.*, 2019; Terrer *et al.*, 2019). Together, the postulated increase in productivity with temperature and precipitation increase could lead to the *greening* of the TMFs in Sikkim Himalaya, at least in the short term

(Sebastian *et al.*, 2019). Similar evidence has already been reported from the wetter parts of eastern Nepal Himalaya, where climate warming and increased summer precipitation are likely to remove moisture constraints on photosynthesis on treeline conifer and broad-leaved species (Pandey *et al.*, 2020). Over longer time scales, the increase in productivity may not necessarily lead to higher carbon sequestration and net carbon gain. In a growth simulation study of 141 temperate tree species, Bugmann and Bigler (2011) show that the higher productivity due to the CO_2 fertilization effect is associated with proportionately lesser biomass gain as well as reduced longevity leading to net zero carbon gains.

Conclusions

It is still challenging to predict plant-water relations in diverse secondary TMFs because of the variability among different functional groups and the diversity in traits that regulate plant-water relations (Huc *et al.*, 1994; Nogueira *et al.*, 2004; Küppers *et al.*, 2008). Regardless, the plant-water relations in these East Himalayan wet tropical montane broad-leaved forests have been estimated for the first-time using methods covering the maximum variability of sap flow using limited resources. Sap flow was 3-9 times higher than their conspecifics in relatively drier Central Himalaya and East Asia, highlighting the interactive role of precipitation and elevation in modulating the available energy, moisture, and plant productivity (Bruijnzeel *et al.*, 2011). Radial and azimuthal probes opened a whole new dimension of understanding plant-water use for Himalayan species, and their use is highly recommended to minimize the errors in estimating whole-tree sap flow (Shinohara *et al.*, 2013; Komatsu *et al.*, 2016). Significant nocturnal sap flow, dominated by the pre-dawn movement, is the first report from the Himalaya and we postulate two potential roles leading to adaptation of the pre-dawn sap flux in the wet energy-limited montane systems: (A) facilitate carbon fixation during cloud-free early-morning hours by ensuring adequate leaf water balance and keeping stomata open, and (B) ensure nutrient and O2 transport for early morning developmental work in the trees. The nocturnal sap flow observations hold significance for future SPAC work in terms of shifting the timing of pre-dawn leaf water potential measurements (Kavanagh *et al.*, 2007), estimating water-use efficiency across species (Chaves *et al.*, 2016), quantifying hydrological services (Siddiq and Cao, 2018; Kangur *et al.*, 2021) and improving regional climate change modelling exercises (De Dios *et al.*, 2015). Other adaptations like midday depression in shallow-rooted pioneer species highlight their sensitivity to environmental extremes (dos Santos *et al.*, 2019).

Studies on climate change in the Eastern Himalaya have predicted an increase in summer rainfall, declining winter rains, and increasing summer and winter temperatures (Kulkarni *et al.*, 2013; Krishnan *et al.*, 2019). Thus, drier and warmer winters are likely to impact the phenology and negatively affect the productivity of shallow-rooted pioneers like *S. racemosa* and *E. acuminata*. In contrast, deep-rooted species like *C. hystrix* and Himalayan oaks may remain unaffected by seasonal droughts (Kumar *et al.*, 2022, Preprint). Thus, the secondary broad-leaved forests, with the dominance of shallow-rooted pioneers, are more prone to the negative impacts of drier and warmer winters than primary forests, which are dominated by deep-rooted species. In the summer, the onset of rain provides enough moisture to ensure peak vegetation productivity in April. However, increased summer precipitation in the future could result in higher cloud cover, negatively impacting both vegetation productivity and transpiration (Donohue *et al.*, 2017), but may also allow the opportunistic fast-growing pioneers to strengthen alongside the late-successional species in short-term (Lyu *et al.*, 2020). The CO_2 fertilization effect could potentially benefit both the species groups but may be limited by the availability of soil nutrients like nitrogen and phosphorus, and any gains are likely to be offset by lower biomass gain and reduced longevity. The net effect of the postulated increase in productivity due to warming, CO_2 fertilization and precipitation increase could lead to the *greening* of the TMFs in Sikkim Himalaya, at least in the short term (Krishnaswamy *et al.*, 2014; Sebastian *et al.*, 2019).

The overall effect of temperature and precipitation changes on the region's biodiversity remains complex and requires ecohydrological models specific to the East Himalayan TMFs. More regional studies, inclusive of diurnal and seasonal variability in transpiration, will be critical for improving the accuracy of land-surface interaction models and predicting the impact of climate change on Himalayan ecohydrology (Wang and Dickinson, 2012; Miller *et al.*, 2018). The study provides the first empirical understanding of climatic controls on vegetation water-use from a wet high elevation tropical broad-leaved evergreen wet montane forest in Eastern Himalaya, one of the 30 global biodiversity hotspots and 200 ecoregions of importance. The GLS model results highlight the interacting roles of R_s and VPD in modulating sap flow and contribute to the scant literature on plant-water relations from secondary TMFs with distinct water use behaviour in contrast to primary forests. It also highlights the pitfalls of generalizing water-use across functional groups, forest types, and climatic conditions (Berdanier *et al.*, 2016) and compares the plant-water use strategies between co-occurring pioneer and late-successional species for accessing changing energy and soil moisture conditions (Bretfeld *et al.*, 2018; Moore *et al.*, 2018). The study recommends prioritizing the conservation and management of these secondary forests in the Eastern Himalaya for sustained ecosystem services.

Supplementary Data

The following supplementary data are available at JXB online.

Fig. S1. Barplots of vegetation distribution in FWS showing (A) tree density of top seven species per hectare and (B) basal area (m^2 ha^{-1}) of the same species.

Fig. S2. Time-series plots of the raw daily data of the SPAC variables from winters (December) to summers (May).

Fig. S3. Variability in sapwood properties along the depth of the xylem.

Fig. S4. Scatterplots showing the relationship between mean hourly sap flux density for 14th December 2013 (when the wood cores were extracted) and (A) Wood moisture (in %) and (B) Wood density (g cm^{-3}) for each sapwood annulus ring in the three species.

Fig. S5. Variability in sap flow across the three species in (A) diurnal patterns in correction factor (C_h, unitless) used as a proxy of radial variability, (B) diurnal patterns in sap flow ratios (R_{NS}, unitless) used as a proxy of azimuthal variability.

Fig. S6. Scatterplots between sap flow (V, kg hr^{-1}) and (A) Incoming short-wave radiation (R_s, kW m^{-2}) and (B) Vapour pressure deficit (VPD, kPa) for the three species.

Fig. S7. Scatterplots between nocturnal sap flow (V_{night} in % of daily V) and (A) Vapour pressure deficit (VPD), (B) Soil moisture (S) and (C) Wind velocity (u) across the three species.

Fig. S8. Radial variability in sap flux density across different seasons is shown by plotting the average daily maximum sap flux density (Daily J_{max}, cm^3 cm^2 hr^{-1}) along the depth of the xylem.

Fig. S9. Boxplots of the percentage contribution of sap flow at different sapwood depths to daily whole-tree sap flow (V, kg hr^{-1}) plotted against different months for the three species.

Fig. S10. Comparison of diurnal patterns in observed and predicted whole-tree sap flow (V, kg hr^{-1}) of (A) *S. racemosa*, (B) *E. acuminata* and (C) *C. hystrix* derived from the Generalized least squares (GLS) linear regression models for the three species.

Table. S1. Slopes (m) and r^2 (in bracket) of the linear regression models without intercept (LRMs) developed for each hour of the day for the three species *S. racemosa*, *E. acuminata*, and *C. hystrix* used for estimating sap flow in replicate trees using equation 3.

Table. S2. Results from multiple linear regression models (MLRMs) for the day (0600-1800 h) and the night (1800-0600 h) periods to assess the drivers of radial variability in sap flow across the three species.

Table. S3. Results from multiple linear regression models (MLRMs) for the day (0600-1800 h) and the night (1800-0600 h) periods to assess the drivers of azimuthal variability across the three species

Table. S4. Results from multiple linear regression models (MLRMs) to assess the drivers of nocturnal sap flow (V_{night}) across the three species.

Acknowledgments

The authors thank the Department of Forests, Environment and Wildlife Management, Rural Management and Development Department, the Home Department, Govt. of Sikkim, India, and the Indian Army for research permits and field support in Sikkim. The study would not have been possible without the crucial field support from Mr. Passang Tamang, Mr. Girish Varma, Mr. Naresh Rai, and the staff of Fambong-Loh Wildlife Sanctuary, East Sikkim. The authors thank Dr. Nachiket Kelkar and Dr. Aniruddha Marathe for their useful comments on the statistical analysis, and Mr. Lalit Kumar Rai and Dr. Radhika Kanade for their valuable insights on forest ecology. The authors are indebted to Prof. Nathan G. Phillips at Boston University, USA, Prof. Frederick Meinzer at Oregon State University, USA, and Forests Science Laboratory (Corvallis), USA, for generously sharing the original thermal dissipation probe assembly design. The authors acknowledge the logistical support provided by ATREE Regional Office, Gangtok, during the study.

Authors' Contributions

Manish Kumar: Conceptualization, Methodology, Manufacturing, Testing and modification of the sap flow probes, Investigation, Software, Formal analysis, Visualization, Writing – Original draft preparations. **Yangchenla Bhutia:** Investigation, Writing – Review & Editing. **Gladwin Joseph:** Conceptualization, Methodology, Testing and modification of the sap flow probes, Writing – Review & Editing. **Jagdish**

Krishnaswamy: Conceptualization, Methodology, Writing – Review & Editing, Supervision, Project Administration, Funding Acquisition.

Conflict of interest

The authors have no relevant financial or non-financial interests to disclose. The authors have no relevant competing interests to disclose

Funding

Department of Biotechnology, Govt. of India (GoI) (Grant No. BT/01/NE/PS/NCBS/09); National Mission for Himalayan Studies (NMHS), Ministry of Environment, Forest and Climate Change, GoI (Grant No: GBPI/NMHS/HF/RA/2015-16/).

Data Availability

The data supporting this study's findings are available on request from the corresponding author. The data are not publicly available due to privacy or ethical restrictions. A sample subset of the data supporting this study's findings is available in Dryad at (doi:10.5061/dryad.47d7wm3cg) under the citation Kumar (2021). The sample dataset is available for preview here: https://datadryad.org/stash/share/bkDWLqnM4S2C3w0wgri1AcXlyDz3eM2Sgs7prOqLZqk

References

Allen MF. 2014. How Oaks Respond to Water Limitation. Gen. Tech. Rep. PSW-GTR-251. Berkeley, CA: US Department of Agriculture, Forest Service, Pacific Southwest Research Station **251**, 13–22.

Aparecido LMT, Miller GR, Cahill AT, Moore GW. 2016. Comparison of tree transpiration under wet and dry canopy conditions in a Costa Rican premontane tropical forest. Hydrological Processes **30**, 5000–5011.

Asbjornsen H, Goldsmith GR, Alvarado-Barrientos MS, *et al.* 2011. Ecohydrological advances and applications in plant-water relations research: A review. Journal of Plant Ecology **4**, 3–22.

Barbeta A, Ogaya R, Peñuelas J. 2012. Comparative study of diurnal and nocturnal sap flow of Quercus ilex and Phillyrea latifolia in a Mediterranean holm oak forest in Prades (Catalonia, NE Spain). Trees - Structure and Function **26**, 1651–1659.

Basnett S, Devy SM. 2021. Phenology determines leaf functional traits across Rhododendron species in the Sikkim Himalaya. Alpine Botany **131**, 63–72.

Berdanier AB, Miniat CF, Clark JS. 2016. Predictive models for radial sap flux variation in coniferous, diffuse-porous and ring-porous temperate trees. Tree Physiology, tpw027.

Berry ZC, Gotsch SG, Holwerda F, Muñoz-Villers LE, Asbjornsen H. 2016. Slope position influences vegetation-atmosphere interactions in a tropical montane cloud forest. Agricultural and Forest Meteorology **221**, 207–218.

Berry ZC, Looker N, Holwerda F, Gómez Aguilar LR, Ortiz Colin P, González Martínez T, Asbjornsen H. 2018. Why size matters: The interactive influences of tree diameter distribution and sap flow parameters on upscaled transpiration. Tree Physiology **38**, 264–276.

Bhutia Y, Gudasalamani R, Ganesan R, Saha S. 2019. Assessing forest structure and composition along the altitudinal gradient in the state of Sikkim, Eastern Himalayas, India. Forests **10**, 1–17.

Bond BJ, Jones J a., Moore G, Phillips N, Post D, McDonnell JJ. 2002. The zone of vegetation influence on baseflow revealed by diel patterns of streamflow and vegetation water use in a headwater basin. Hydrological Processes **16**, 1671–1677.

Bretfeld M, Ewers BE, Hall JS. 2018. Plant water use responses along secondary forest succession during the 2015–2016 El Niño drought in Panama. New Phytologist **219**, 885–899.

Brodersen CR, Roddy AB, Wason JW, McElrone AJ. 2019. Functional Status of Xylem Through Time. Annual Review of Plant Biology **70**, 1–27.

Brown S, Hall M, Gregory W, Lugo AE. 2019. Tropical Secondary Forests. **6**, 1–32.

Bruijnzeel LA, Mulligan M, Scatena FN. 2011. Hydrometeorology of tropical montane cloud forests: Emerging patterns. Hydrological Processes **25**, 465–498.

Bugmann H, Bigler C. 2011. Will the CO2 fertilization effect in forests be offset by reduced tree longevity? Oecologia **165**, 533–544.

Burgess SSO, Dawson TE. 2008. Using branch and basal trunk sap flow measurements to estimate whole-plant water capacitance: A caution. Plant and Soil **305**, 5–13.

Carminati A, Passioura JB, Zarebanadkouki M, Ahmed MA, Ryan PR, Watt M, Delhaize E. 2017. Root hairs enable high transpiration rates in drying soils. New Phytologist, 771–781.

Čermák J, Nadezhdina N. 2011. Instrumental approaches for studying tree-water relations along gradients of tree size and forest age. In: Meinzer F,, In: Lachenbruch B,, In: Dawson T, eds. Size- and Age-Related Changes in Tree Structure and Function. Tree Physiology. Springer, Dordrecht, 385–426.

Chan AM, Bowling DR. 2017. Assessing the thermal dissipation sap flux density method for monitoring cold season water transport in seasonally snow-covered forests. Tree Physiology **37**, 984–995.

Chand DB, Poudyal K, Jha PK. 2017. SHIFTS IN LEAF PHENOLOGY OF THREE HIMALAYAN OAK SPECIES: ROLE OF WOOD WATER PROPERTIES. ECOPRINT, 29–36.

Chave J. 2006. *Measuring wood density for tropical forest trees: a field manual*.

Chaves MM, Costa JM, Zarrouk O, Pinheiro C, Lopes CM, Pereira JS. 2016. Controlling stomatal aperture in semi-arid regions—The dilemma of saving water or being cool? Plant Science **251**, 54–64.

Chen X, Gao J, Zhao P, McCarthy HR, Zhu L, Ni G, Ouyang L. 2018. Tree species with photosynthetic stems have greater nighttime sap flux. Frontiers in Plant Science **9**, 1–9.

Chettri N, Sharma E, Deb DC, Sundriyal RC. 2002. Impact of firewood extraction on tree structure, regeneration and woody biomass productivity in a trekking corridor of the Sikkim Himalaya. Mountain Research and Development **22**, 150–158.

Chiariello NR, Field CB, Mooney HA. 2006. Midday Wilting in a Tropical Pioneer Tree. Functional Ecology **1**, 3.

Chiu CW, Komatsu H, Katayama A, Otsuki K. 2016. Scaling-up from tree to stand transpiration for a warm-temperate multi-specific broadleaved forest with a wide variation in stem diameter. Journal of Forest Research **21**, 161–169.

Chu CR, Hsieh CI, Wu SY, Phillips NG. 2009. Transient response of sap flow to wind speed. Journal of Experimental Botany **60**, 249–255.

Dahal N, Lamichhaney S, Kumar S. 2021. Climate Change Impacts on Himalayan Biodiversity:

Evidence-Based Perception and Current Approaches to Evaluate Threats Under Climate Change. Journal of the Indian Institute of Science **101**, 195–210.

Daniel D, Anandhi A, Sen S. 2021. Conceptual model for the vulnerability assessment of springs in the indian himalayas. Climate **9**, 1–20.

Davis TW, Kuo C-M, Liang X, Yu P-S. 2012. Sap Flow Sensors: Construction, Quality Control and Comparison. Sensors **12**, 954–971.

Delzon S, Sartore M, Granier A, Loustau D. 2004. Radial profiles of sap flow with increasing tree size in maritime pine. Tree physiology **24**, 1285–1293.

Dimri AP, Kumar D, Srivastava M. 2018. Regional Climate Changes over Northeast India: Present and Future. In: Singh A,, In: Punia M,, In: Haran N,, In: Singh T, eds. Development and Disaster Management. Palgrave Macmillan, Singapore, .

De Dios VR, Roy J, Ferrio JP, Alday JG, Landais D, Milcu A, Gessler A. 2015. Processes driving nocturnal transpiration and implications for estimating land evapotranspiration. Scientific Reports **5**, 1–8.

Dong T, Duan B, Korpelainen H, Niinemets Ü, Li C. 2019. Asymmetric pruning reveals how organ connectivity alters the functional balance between leaves and roots of Chinese fir. Journal of Experimental Botany **70**, 1941–1953.

Donohue RJ, Roderick ML, McVicar TR. 2007. On the importance of including vegetation dynamics in Budyko's hydrological model. Hydrology and Earth System Sciences **11**, 983–995.

Donohue RJ, Roderick ML, McVicar TR, Yang Y. 2017. A simple hypothesis of how leaf and canopy-level transpiration and assimilation respond to elevated CO2 reveals distinct response patterns between disturbed and undisturbed vegetation. Journal of Geophysical Research: Biogeosciences **122**, 168–184.

Eckert D, Martens HJ, Gu L, Jensen AM. 2021. CO2 refixation is higher in leaves of woody species with high mesophyll and stomatal resistances to CO2 diffusion. Tree Physiology **41**, 1450–1461.

Fiora A, Cescatti A. 2006. Diurnal and seasonal variability in radial distribution of sap flux density: Implications for estimating stand transpiration. Tree Physiology **26**, 1217–1225.

Flo V, Martinez-Vilalta J, Steppe K, Schuldt B, Poyatos R. 2019. A synthesis of bias and uncertainty in sap flow methods. Agricultural and Forest Meteorology **271**, 362–374.

Forrester DI. 2015. Transpiration and water-use efficiency in mixed-species forests versus monocultures: Effects of tree size, stand density and season. Tree Physiology **35**, 289–304.

Forster MA. 2014. How significant is nocturnal sap flow? Tree Physiology **34**, 757–765.

Franco AC, Lüttge U. 2002. Midday depression in savanna trees: Coordinated adjustments in photochemical efficiency, photorespiration, CO2 assimilation and water use efficiency. Oecologia **131**, 356–365.

Gao J, Zhao P, Shen W, Niu J, Zhu L, Ni G. 2015. Biophysical limits to responses of water flux to vapor pressure deficit in seven tree species with contrasting land use regimes. Agricultural and Forest Meteorology **200**, 258–269.

Ghimire CP, Lubczynski MW, Bruijnzeel LA, Chavarro-Rincón D. 2014. Transpiration and canopy conductance of two contrasting forest types in the Lesser Himalaya of Central Nepal. Agricultural and Forest Meteorology **197**, 76–90.

Granier A. 1987. Evaluation of transpiration in a Douglas-fir stand by means of sap flow measurements. Tree physiology **3**, 309–20.

Gupta HV, Kling H. 2011. On typical range, sensitivity, and normalization of Mean Squared Error and Nash-Sutcliffe Efficiency type metrics. Water Resources Research **47**, 2–4.

Gurung S, Chettri A. 2019. Vegetation analysis of Oak Forests of Fambong lho Wildlife Sanctuary in Sikkim Himalayas. Researchgate.Net **6**, 192–197.

Guyot A, Ostergaard KT, Fan J, Santini NS, Lockington DA. 2015. Xylem hydraulic properties in subtropical coniferous trees influence radial patterns of sap flow: implications for whole tree transpiration estimates using sap flow sensors. Trees - Structure and Function **29**, 961–972.

Harmon T. 2009. Sap-Happy Sap flow probe construction and use. 2009 PASI-PASEO Course Reading And Presentations, 1–9.

Hashimoto H, Nemani RR, Bala G, *et al.* 2019. Constraints to vegetation growth reduced by region-specific changes in seasonal climate. Climate **7**.

Hatton TJ, Catchpole EA, Vertessy RA. 1990. Integration of sap flow velocity to estimate plant water use. Tree Physiology **6**, 201–209.

Heimann M, Reichstein M. 2008. Terrestrial ecosystem carbon dynamics and climate feedbacks. Nature **451**, 289–292.

Hernandez-Santana V, Hernandez-Hernandez A, Vadeboncoeur MA, Asbjornsen H. 2015. Scaling from single-point sap velocity measurements to stand transpiration in a multispecies deciduous forest: uncertainty sources, stand structure effect, and future scenarios. Canadian Journal of Forest Research **45**, 1489–1497.

Huc R, Ferhi A, Guehl JM. 1994. Pioneer and late stage tropical rainforest tree species (French Guiana) growing under common conditions differ in leaf gas exchange regulation, carbon isotope discrimination and leaf water potential. Oecologia **99**, 297–305.

James S a, Clearwater MJ, Meinzer FC, Goldstein G. 2002. Heat dissipation sensors of variable length for the measurement of sap flow in trees with deep sapwood. Tree physiology **22**, 277–283.

Kamakura M, Tsuruta K, Azuma WA, Kosugi Y. 2021. Hydraulic architecture and internal water storage of Japanese cypress using measurements of sap flow and water potential. Ecohydrology **14**, 1–6.

Kambach S, Condit R, Aguilar S, *et al.* 2022. Consistency of demographic trade-offs across 13 (sub)tropical forests. Journal of Ecology **110**, 1485–1496.

Kanade R, John R. 2018. Topographical influence on recent deforestation and degradation in the Sikkim Himalaya in India; Implications for conservation of East Himalayan broadleaf forest. Applied Geography **92**, 85–93.

Kangur O, Steppe K, Schreel JDM, Von Der Crone JS, Sellin A. 2021. Variation in nocturnal stomatal conductance and development of predawn disequilibrium between soil and leaf water potentials in nine temperate deciduous tree species. Functional Plant Biology **48**, 483–492.

Kannenberg SA, Guo JS, Novick KA, Anderegg WRL, Feng X, Kennedy D, Konings AG, Martínez-Vilalta J, Matheny AM. 2022. Opportunities, challenges and pitfalls in characterizing plant water-use strategies. Functional Ecology **36**, 24–37.

Kavanagh KL, Pangle R, Schotzko AD. 2007. Nocturnal transpiration causing disequilibrium between soil and stem predawn water potential in mixed conifer forests of Idaho. Tree Physiology.621–629.

Kim HK, Park J, Hwang I. 2014. Investigating water transport through the xylem network in vascular plants. Journal of Experimental Botany **65**, 1895–1904.

Komatsu H, Shinohara Y, Kume T, Tsuruta K, Otsuki K. 2016. Does measuring azimuthal variations in sap flux lead to more reliable stand transpiration estimates? Hydrological Processes, n/a-n/a.

Krishnan R, Shrestha AB, Ren G, *et al.* 2019. Unravelling Climate Change in the Hindu Kush Himalaya: Rapid Warming in the Mountains and Increasing Extremes. In: Wester P,, In: Mishra A,, In: Mukherji A,, In: Shrestha AB,, In: Change C, eds. The Hindu Kush Himalaya Assessment. Springer International Publishing, .

Krishnaswamy J, Bonell M, Venkatesh B, Purandara BK, Lele S, Kiran MC, Reddy V, Badiger S, Rakesh KN. 2012. The rain-runoff response of tropical humid forest ecosystems to use and reforestation in the western ghats of India. Journal of Hydrology **472–473**, 216–237.

Krishnaswamy J, John R, Joseph S. 2014. Consistent response of vegetation dynamics to recent climate change in tropical mountain regions. Global Change Biology **20**, 203–215.

Kulkarni A, Patwardhan S, Kumar KK, Ashok K, Krishnan R. 2013. High-resolution Regional Climate Model PRECIS Projected Climate Change in the Hindu Kush – Himalayan Region By Using the High-resolution Regional Climate Model PRECIS. Mountain Research and Development **33**, 142–151.

Kumagai T, Aoki S, Shimizu T, Otsuki K. 2007. Sap flow estimates of stand transpiration at two slope positions in a Japanese cedar forest watershed. Tree physiology **27**, 161–8.

Kumar M, Bhutia Y, Joseph G, Krishnaswamy J. 2022. Transpiration drives diurnal and seasonal streamflow in secondary tropical montane forests of Eastern Himalaya. Authorea, Preprint, December 08, 2022, 1–22.

Kumar M, Hodnebrog Ø, Sophie Daloz A, Sen S, Badiger S, Krishnaswamy J. 2021. Measuring precipitation in Eastern Himalaya: Ground validation of eleven satellite, model and gauge interpolated gridded products. Journal of Hydrology **599**.

Kumar M, Rathod R, Mukherji A. 2023. Water security and spring conservation in the Himalaya. In: Ojha H,, In: Schofield N,, In: Camkin J, eds. Climate Risks to Water Security: Framing Effective Response in Asia and the Pacific. Palgrave Macmillan, Singapore, 1–21.

Küppers M, Motzer T, Schmitt D, Ohlemacher C, Zimmermann R, Horna V, Küppers BIL, Mette T. 2008. Stand Structure, Transpiration Responses in Trees and Vines and Stand Transpiration of Different Forest Types Within the Mountain Rainforest. Gradients in a Tropical Mountain Ecosystem of Ecuador.149–156.

Lai HR, Craven D, Hall JS, Hui FKC, van Breugel M. 2021. Successional syndromes of saplings in tropical secondary forests emerge from environment-dependent trait–demography relationships. Ecology Letters **24**, 1776–1787.

Li Y, Liu J, Chen G, Zhou G, Huang W, Yin G, Zhang D, Li Y. 2013. Water-use efficiency of four native trees under CO2 enrichment and N addition in subtropical model forest ecosystems. Journal of Plant Ecology **8**, 411–419.

Lu P, Urban L, Ping Z. 2004. Granier's Thermal Dissipation Probe (TDP) Method for Measuring Sap Flow in Trees : Theory and Practice. Acta Botanica Sinica **46**, 631–646.

Lyu J, He QY, Yang J, Chen QW, Cheng RR, Yan MJ, Yamanaka N, Du S. 2020. Sap flow characteristics in growing and non-growing seasons in three tree species in the semiarid Loess Plateau region of China. Trees - Structure and Function **34**, 943–955.

Manzoni S, Vico G, Porporato A, Katul G. 2013. Biological constraints on water transport in the soil–plant–atmosphere system. Advances in Water Resources **51**, 292–304.

Marks CO, Lechowicz M. 2007. The ecological and functional correlates of nocturnal transpiration. Tree Physiology **27**, 577–584.

McCulloh KA, Meinzer FC, Sperry JS, Lachenbruch B, Voelker SL, Woodruff DR, Domec JC. 2011. Comparative hydraulic architecture of tropical tree species representing a range of successional stages and wood density. Oecologia **167**, 27–37.

Mcvicar TR, Donohue RJ, Grady APO, Li L. 2010. *The effects of climatic changes on plant physiological and catchment ecohydrological processes in the high-rainfall catchments of the Murray-Darling Basin : A scoping study*.

Mencuccini M, Manzoni S, Christoffersen B. 2019. Modelling water fluxes in plants: from tissues to biosphere. New Phytologist **222**, 1207–1222.

Mengis N, Keller DP, Eby M, Oschlies A. 2015. Uncertainty in the response of transpiration to CO2 and implications for climate change. Environmental Research Letters **10**.

Miller G, Cahill T, Moore G, Leung R. 2018. Improving Land - Surface Modeling of Evapotranspiration Processes in Tropical Forests. (No. DOE-TAMU-10654) Texas A&M Engineering Experiment Station, 77843.

Moore GW, Jones JA, Bond BJ. 2011. How soil moisture mediates the influence of transpiration on streamflow at hourly to interannual scales in a forested catchment. Hydrological Processes **25**, 3701–3710.

Moore GW, Orozco G, Aparecido LMT, Miller GR. 2018. Upscaling transpiration in diverse forests: Insights from a tropical premontane site. Ecohydrology **11**, 1–13.

Motzer T, Munz N, Anhuf D, Küppers M. 2010. Transpiration and microclimate of a tropical montane rain forest, southern Ecuador. In: Bruijnzeel L. A., Scatena F. N. HLS, ed. Tropical Montane Cloud Forests: Science for Conservation and Management. Cambridge University Press, 447–455.

Motzer T, Munz N, Küppers M, Schmitt D, Anhuf D. 2005. Stomatal conductance, transpiration and sap flow of tropical montane rain forest trees in the southern Ecuadorian Andes. Tree Physiology **25**, 1283–1293.

Nachabe M, Shah N, Ross M, Vomacka J. 2005. Evapotranspiration of Two Vegetation Covers in a Shallow Water Table Environment. Soil Science Society of America Journal **69**, 492.

Nogueira A, Martinez CA, Ferreira LL, Prado CHBA. 2004. Photosynthesis and water use efficiency in twenty tropical tree species of differing succession status in a Brazilian reforestation. Photosynthetica **42**, 351–356.

O'Brien JJ, Oberbauer SF, Clark DB. 2004. Whole tree xylem sap flow responses to multiple environmental variables in a wet tropical forest. Plant, Cell and Environment **27**, 551–567.

Ohsawa M. 1993. Latitudinal pattern of mountain vegetation zonation in southern and eastern Asia. Journal of Vegetation Science **4**, 13–18.

Ohsawa M, Shakya PR, Numata M. 1986. Distribution and succession of West Himalayan forest types in the eastern part of the Nepal Himalaya. Mountain Research & Development **6**, 143–157.

Pandey S, Cherubini P, Saurer M, Carrer M, Petit G. 2020. Effects of climate change on treeline trees in Sagarmatha (Mt. Everest, Central Himalaya). Journal of Vegetation Science **31**, 1146–1155.

Paudel I, Kanety T, Cohen S. 2013. Inactive xylem can explain differences in calibration factors for thermal dissipation probe sap flow measurements. Tree Physiology **33**, 986–1001.

Pausch RC, Grote EE, Dawson TE. 2000. Estimating water use by sugar maple trees: considerations when using heat-pulse methods in trees with deep functional sapwood. Tree physiology **20**, 217–227.

Pavlis J, Jeník J. 2000. Roots of pioneer trees in amazonian rain forest. Trees - Structure and Function **14**, 442–455.

Peters RL, Fonti P, Frank DC, *et al.* 2018. Quantification of uncertainties in conifer sap flow measured with the thermal dissipation method. New Phytologist **219**, 1283–1299.

Phillips N, Nagchaudhuri A, Oren R, Katul G. 1997. Time constant for water transport in loblolly pine trees estimated from time series of evaporative demand and stem sapflow. Trees - Structure and Function **11**, 412–419.

Phillips N, Oren R, Zimmermann R. 1996. Radial patterns of xylem sap flow in non-, diffuse- and ring-porous tree species. Plant, Cell and Environment **19**, 983–990.

Pinheiro JC, Bates D. 2006. Mixed-Effects Models in S and S-PLUS. Springer Science & Business Media, 250–270.

Poudyal K, Jha PK, Zobel DB, Thapa CB. 2004. Patterns of leaf conductance and water potential of five Himalayan tree species. Tree physiology **24**, 689–99.

Poyatos R, Granda V, Flo V, Adams MA, Adorján B, Aguadé D, Aidar MPM, Allen S, Alvarado-barrientos MS, Anderson-teixeira KJ. 2021. Global transpiration data from sap flow measurements: the SAPFLUXNET database. Earth System Science Data Discussions **13**, 2607–2649.

R Core Team. 2022. R: A language and environment for statistical computing. R Foundation for Statistical Computing, Vienna, Austria.

Ramakrishnan PS, Kushwaha SPS. 2001. Secondary forests of the Himalaya with emphasis on the north-eastern hill region of India. Journal of Tropical Forest Science, 727–747.

Resco de Dios V, Díaz-Sierra R, Goulden ML, Barton CVM, Boer MM, Gessler A, Ferrio JP, Pfautsch S, Tissue DT. 2013. Woody clockworks: Circadian regulation of night-time water use in Eucalyptus globulus. New Phytologist **200**, 743–752.

Rüger N, Condit R, Dent DH, DeWalt SJ, Hubbell SP, Lichstein JW, Lopez OR, Wirth C,

Farrior CE. 2020. Demographic trade-offs predict tropical forest dynamics. Science **368**, 165–168.

dos Santos O de O, Mendes KR, Martins SVC, Batista-Silva W, dos Santos MA, de Figueirôa JM, de Souza ER, Fernandes D, Araújo WL, Pompelli MF. 2019. Physiological parameters and plasticity as key factors to understand pioneer and late successional species in the Atlantic Rainforest. Acta Physiologiae Plantarum **41**, 1–18.

Schaap MG, Leij FJ, Van Genuchten MT. 2001. Rosetta: A computer program for estimating soil hydraulic parameters with hierarchical pedotransfer functions. Journal of Hydrology **251**, 163–176.

Sebastian DE, Ganguly S, Krishnaswamy J, Du K, Nemani R, Ghosh S. 2019. Multi-Scale Association between Vegetation Growth and Climate in India : A Wavelet Analysis Approach. Remote Sensing **11**, 2073.

Sharma A, Goyal MK. 2020. Assessment of the changes in precipitation and temperature in Teesta River basin in Indian Himalayan Region under climate change. Atmospheric Research **231**, 104670.

Sharma CL, Sharma M, Carter MJ, Kharkongor BM. 2011. Inter species wood variation of Castanopsis species of Meghalaya. Journal of the Indian Academy of Wood Science **8**, 124–129.

Shinohara Y, Tsuruta K, Ogura A, Noto F, Komatsu H, Otsuki K, Maruyama T. 2013. Azimuthal and radial variations in sap flux density and effects on stand-scale transpiration estimates in a Japanese cedar forest. Tree Physiology **33**, 550–558.

Shrestha UB, Gautam S, Bawa KS. 2012. Widespread climate change in the Himalayas and associated changes in local ecosystems. PloS one **7**, e36741.

Siddiq Z, Cao KF. 2018. Nocturnal transpiration in 18 broadleaf timber species under a tropical seasonal climate. Forest Ecology and Management **418**, 47–54.

Singh SP, Bassignana-Khadka I, Karky BS, Sharma E, Eklabya S, Sharma E. 2011. *Climate change in the Hindu Kush-Himalayas: the state of current knowledge*. International Centre for Integrated Mountain Development (ICIMOD).

Singh SP, Tewari A, Singh SK, Pathak GC. 2000. Significance of phenologically asynchronous populations of the central Himalayan oaks in drought adaptation. Current Science **79**, 353–357.

Singh S, Zobel D, Garkoti S. 2006*a*. Patterns in water relations of central Himalayan trees. Tropical … **47**, 159–182.

Singh SP, Zobel DB, Garkoti SC, Tewari A, Negi CMS. 2006*b*. Patterns in water relations of central Himalayan trees. Tropical Ecology **47**, 159–182.

Sobrado MA. 2003. Hydraulic characteristics and leaf water use efficiency in trees from tropical montane habitats. Trees - Structure and Function **17**, 400–406.

Sudhakar S, Prasad PRC, Arrawatia ML, Sudha K, Babar S, Rajeshwar Rao SKSV. 2008. Landscape analysis in Fambong Lho wildlife sanctuary, east district, Sikkim, India using remote sensing and GIS techniques. Journal of the Indian Society of Remote Sensing **36**, 203–216.

Sundriyal RC, Sharma E. 1996. Anthropogenic pressure on tree structure and biomass in the temperate forest of Mamlay watershed in Sikkim. Forest Ecology and Management **81**, 113–134.

Sundriyal RC, Sharma E. 2003. Underutilized edible plants of the Sikkim Himalaya: Need for domestication. Current Science **85**, 731–736.

Suzuki M, Noshiro S, Takahashi A, Yoda K, Joshi L. 1991. WOOD STRUCTURE OF HIMALAYAN PLANTS , II. In: Ohba H,, In: Malla SB, eds. The Himalayan Plants Volume 2. Tokio: The University Museum, The University of Tokyo, 1–118.

Tanaka K, Takizawa H, Kume T, Xu J, Tantasirin C, Suzuki M. 2004. Impact of rooting depth and soil hydraulic properties on the transpiration peak of an evergreen forest in northern Thailand in the late dry season. Journal of Geophysical Research D: Atmospheres **109**, 1–10.

Tang CQ, Ohsawa M. 1999. Altitudinal distribution of evergreen broad-leaved trees and their leaf-size pattern on a humid subtropical mountain, Mt. Emei, Sichuan, China. Plant Ecology **145**, 221–233.

Terrer C, Jackson RB, Prentice IC, *et al.* 2019. Nitrogen and phosphorus constrain the CO2 fertilization of global plant biomass. Nature Climate Change **9**, 684–689.

Tewari A, Bhatt J, Mittal A. 2016. Influence of tree water potential in inducing flowering in Rhododendron arboreum in the central Himalayan region. IForest **9**, 842–846.

Tewari A, Shah S, Singh N, Mittal A. 2018. Treeline species in western himalaya are not water stressed: A comparison with low elevation species. Tropical Ecology **59**, 313–325.

Wang K, Dickinson RE. 2012. A review of global terrestrial evapotranspiration: Observation, modeling, climatology, and climatic variability. Reviews of Geophysics **50**, 1–54.

Wang Q, Gao J, Zhao P, Zhu L, Ouyang L, Ni G, Zhao X. 2018. Biotic- and abiotic-driven variations of the night-time sap flux of three co-occurring tree species in a low subtropical secondary broadleaf forest. AoB PLANTS **10**, 1–13.

Wang H, He K, Li R, Sheng Z, Tian Y, Wen J, Chang B. 2017. Impact of time lags on diurnal estimates of canopy transpiration and canopy conductance from sap-flow measurements of Populus cathayana in the Qinghai–Tibetan Plateau. Journal of Forestry Research **28**, 481–490.

Wang J, Turner NC, Feng H, Dyck M, He H. 2023. Heat tracer-based sap flow methods for tree transpiration measurements: a mini review and bibliometric analysis. Journal of Experimental Botany **74**, 723–742.

Wiedemann A, Marañón-Jiménez S, Rebmann C, Herbst M, Cuntz M. 2016. An empirical study

of the wound effect on sap flux density measured with thermal dissipation probes. Tree Physiology **36**, 1471–1484.

Wohl E, Barros A, Brunsell N, *et al.* 2012. The hydrology of the humid tropics. Nature Climate Change **2**, 655–662.

Yang Y, Donohue RJ, McVicar TR, Roderick ML, Beck HE. 2016. Long-term CO 2 fertilization increases vegetation productivity and has little effect on hydrological partitioning in tropical rainforests. Journal of Geophysical Research: Biogeosciences **121**, 2125–2140.

Zeppel MJB, Lewis JD, Medlyn B, *et al.* 2011. Interactive effects of elevated CO2 and drought on nocturnal water fluxes in Eucalyptus saligna. Tree Physiology **31**, 932–944.

Zeppel M, Macinnis-Ng CMO, Ford CR, Eamus D. 2008. The response of sap flow to pulses of rain in a temperate Australian woodland. Plant and Soil **305**, 121–130.

Zhang Z, Sun G, Chen L, Xu H, Chen S. 2020. Biophysical controls on nocturnal sap flow in plantation forests in a semi-arid region of northern China. Agricultural and Forest Meteorology **284**.

Zhang X, Wang Y, Wang Y, Zhang S, Zhao X. 2019. Effects of social position and competition on tree transpiration of a natural mixed forest in Chongqing, China. Trees - Structure and Function **0**, 0.

Zhang Z, Zhao P, Zhao X, Zhou J, Zhao P, Zeng X, Hu Y, Ouyang L. 2018. The tree height-related spatial variances of tree sap flux density and its scale-up to stand transpiration in a subtropical evergreen broadleaf forest. Ecohydrology **11**, 1–12.

Zobel DB, Garkoti SC, Singh SP, Tewari A, Negi CMS. 2001. Patterns of water potential among forest types of the central Himalaya. Current Science **80**, 774–779.

Tables

Table 1. Life-forms and ecophysiological characteristics of the three species.

Species	**Family**	**Form**	**Functional group**	**Canopy position**	**Rooting depth**	**Wood type**
S. racemosa	Symplocaceae	Small-medium trees	Pioneers	In-canopy	Shallow	Diffuse-porous
E. acuminata	Pentaphylacaceae	Shrubs-small trees	Pioneers	In-canopy	Shallow	Diffuse-porous
C. hystrix	Fagaceae	Large trees	Late-successional	Emergent	Deep	Semi ring-porous

Table 2. Biometric details (± standard deviation) along with the total number of data days and the number of radial probes installed per species.

Species	No. of trees	DBH (m)	Basal area per tree (m^2)	Sapwood area per tree (m^2)	No. of radial probes per tree	Data (days)
S. racemosa	5	0.21 ± 0.06	0.036 ± 0.02	0.032 ± 0.02	5	49
E. acuminata	5	0.19 ± 0.04	0.028 ± 0.01	0.026 ± 0.01	4	87
C. hystrix	3	0.34 ± 0.2	0.11 ± 0.12	0.037 ± 0.02	5	99

Table 3. Estimates of sap flux density (J), whole-tree sap flow (V), tree-to-tree coefficient of variation in sap flow (COV) in the studied species. Percentage biases in whole-tree sap flow (V) estimation due to ignoring radial and azimuthal variability (standard deviation in parentheses) are presented across species.

Species	**J** ($cm^3\ cm^2\ hr^{-1}$)	**V** ($kg\ hr^{-1}$)	**Radial bias** (%)	**Azimuthal bias** (%)
S. racemosa	28 (2)	2.4 (1.2)	8 (4)	-5 (12)
E. acuminata	21 (10)	1.52 (0.8)	1 (3)	5 (12)
C. hystrix	13 (5)	2.39 (1.7)	8 (7)	-21 (41)

Table 4: Percentage contribution of day, night, evening and pre-dawn sap flow to total daily sapflow in the three species (values in %, standard deviation in parentheses).

Species	Day (0600-1700)	Night (1800-0500)	Evening (1800-2300)	Pre-dawn (0000-0500)
S. racemosa	88.7 (7)	11.3 (7)	5.1 (5)	6.2 (7)
E. acuminata	82.8 (9)	17.2 (9)	9.5 (8)	7.7 (7)
C. hystrix	86.5 (5)	13.5 (5)	9.7 (5)	3.8 (4)

Table 5. Results from Generalized least squares (GLS) linear regression model with corARMA correlational structure for whole-tree sap flow in the individual trees of *S. racemosa*, *E. acuminata* and *C. hystrix* (*$P < 0.05$, ** $P < 0.01$, *** $P < 0.001$). Predictor variables include Incoming short-wave radiation (R_s, kW m^{-2}), Vapour Pressure Deficit (VPD, kPa), and Soil moisture (S, mm).

Species	Tree	Season	No. of days	Variables	Coefficients	Std. Error	t-value	p-value
S. racemosa	Tree 2	Summer	9	(Intercept)	0.369	0.09	4.092	0***
				S	0.014	0.067	0.204	0.839
				R_s	-0.337	0.561	-0.601	0.548
				VPD	**1.768**	**0.883**	**2.002**	**0.047***
	Tree 3	Winter	5	(Intercept)	1.164	0.447	2.605	0.01**
				S	-0.159	3.502	-0.045	0.964
				R_s	-0.41	1.715	-0.239	0.812
				VPD	6.832	7.653	0.893	0.374
		Summer	8	(Intercept)	0.564	0.058	9.703	0***
				S	0.041	0.041	1.013	0.312
				R_s	0.413	0.362	1.142	0.255
				VPD	**3.481**	**0.554**	**6.283**	**0***
	Tree 4	Summer	8	(Intercept)	0.255	0.052	4.905	0***
				S	0.016	0.033	0.506	0.614
				R_s	0.014	0.223	0.061	0.952
				VPD	**1.199**	**0.358**	**3.348**	**0.001*****
	Tree 5	Summer	8	(Intercept)	0.14	0.023	5.954	0***
				S	0.009	0.016	0.586	0.559
				R_s	0.148	0.122	1.217	0.225
				VPD	**0.619**	**0.189**	**3.282**	**0.001*****
E. acuminata	Tree 2	Summer	8	(Intercept)	0.146	0.025	5.901	0***
				S	0.004	0.018	0.216	0.829
				R_s	0.165	0.134	1.235	0.219
				VPD	**0.643**	**0.204**	**3.16**	**0.002****
	Tree 3	Summer	9	(Intercept)	0.186	0.057	3.269	0.001***
				S	0.001	0.043	0.016	0.987
				R_s	-0.052	0.36	-0.146	0.884
				VPD	0.297	0.562	0.528	0.598
	Tree 4	Winter	16	(Intercept)	0.342	0.045	7.606	0***
				S	0.169	0.091	1.86	0.064
				R_s	**0.56**	**0.082**	**6.793**	**0***
				VPD	**3.128**	**0.268**	**11.669**	**0***
		Summer	5	(Intercept)	0.869	0.474	1.836	0.069
				S	-0.01	0.317	-0.032	0.974
				R_s	-1.903	1.329	-1.432	0.155
				VPD	0.901	2.984	0.302	0.763
C. hystrix	Tree 1	Winter	9	(Intercept)	0.48	0.128	3.745	0***
				S	0.716	0.3	2.384	0.018*
				R_s	**3.18**	**0.347**	**9.165**	**0***
				VPD	**4.993**	**0.842**	**5.927**	**0***
			16	(Intercept)	0.917	0.121	7.55	0***
				S	-0.395	0.455	-0.868	0.386
				R_s	**1.59**	**0.365**	**4.358**	**0***
				VPD	**11.087**	**1.298**	**8.541**	**0***
		Summer	13	(Intercept)	1.518	0.179	8.489	0***
				S	0.1	0.063	1.591	0.113
				R_s	**2.443**	**0.417**	**5.857**	**0***

			VPD	**8.324**	**0.875**	**9.517**	**0*** **
		10	(Intercept)	1.994	0.376	5.299	0***
			S	0.105	0.164	0.639	0.523
			R_s	0.3	0.44	0.684	0.495
			VPD	**7.807**	**1.191**	**6.555**	**0*** **
Tree 2	Winter	9	(Intercept)	1.484	0.341	4.346	0***
			S	0.75	1.359	0.552	0.581
			R_s	2.1	1.411	1.488	0.138
			VPD	**14.652**	**3.383**	**4.331**	**0*** **
		16	(Intercept)	2.006	0.09	22.228	0***
			S	-0.076	0.503	-0.152	0.879
			R_s	**5.618**	**0.364**	**15.417**	**0*** **
			VPD	**6.347**	**1.381**	**4.596**	**0*** **
	Summer	7	(Intercept)	3.072	0.795	3.863	0***
			S	0.174	0.706	0.246	0.806
			R_s	**-9.826**	**3.332**	**-2.949**	**0.004** **
			VPD	**21.676**	**6.44**	**3.366**	**0.001*** **
Tree 3	Winter	5	(Intercept)	0.865	0.362	2.392	0.018*
			S	0.559	1.456	0.384	0.702
			R_s	0.211	1.398	0.151	0.88
			VPD	4.181	3.218	1.299	0.196
		9	(Intercept)	0.725	0.072	10.015	0***
			S	-0.065	0.18	-0.358	0.72
			R_s	**1.447**	**0.125**	**11.541**	**0*** **
			VPD	**5.374**	**0.408**	**13.171**	**0*** **
	Summer	6	(Intercept)	1.248	0.312	4.007	0***
			S	-0.141	0.199	-0.71	0.479
			R_s	**3.879**	**0.862**	**4.5**	**0*** **
			VPD	0.52	1.757	0.296	0.768

Figure 1

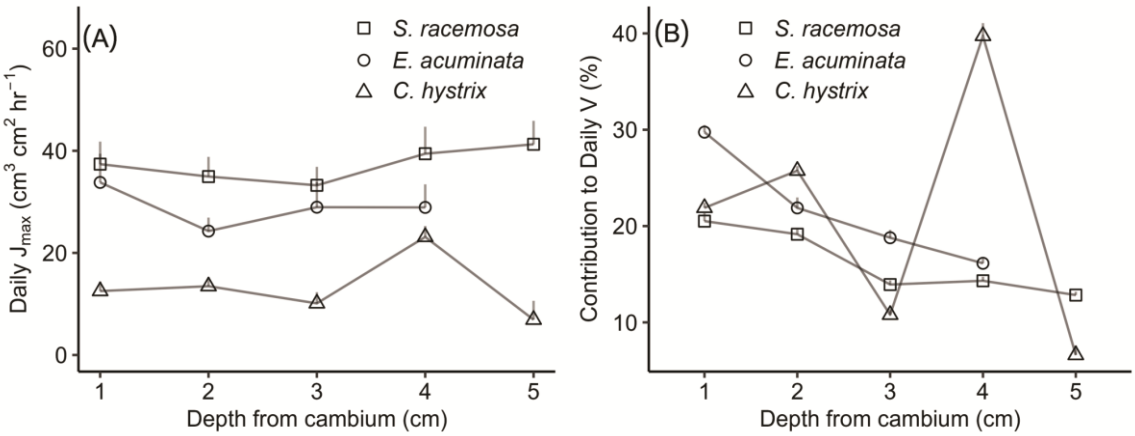

Figure 2

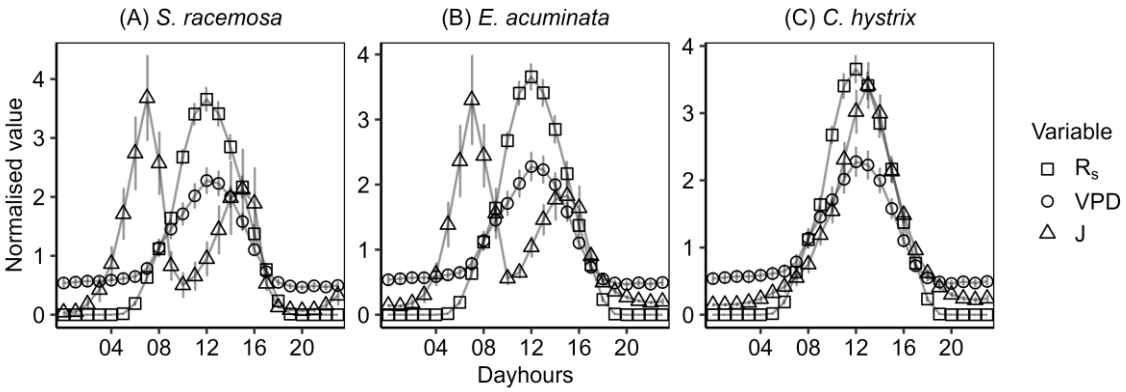

Figure 3

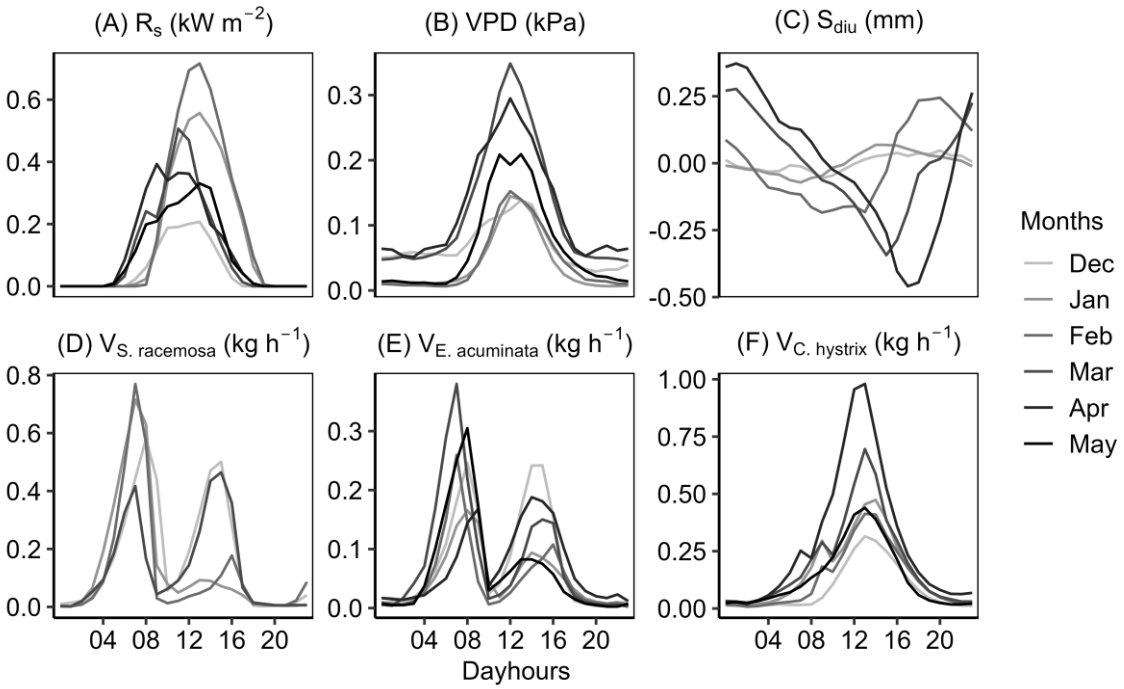

Figure 4